INTERNATIONAL ATOMIC ENERGY AGENCY
UNITED NATIONS EDUCATIONAL, SCIENTIFIC AND CULTURAL ORGANIZATION
INTERNATIONAL CENTRE FOR THEORETICAL PHYSICS
I.C.T.P., P.O. BOX 586, 34100 TRIESTE, ITALY, CABLE: CENTRATOM TRIESTE

UNITED NATIONS INDUSTRIAL DEVELOPMENT ORGANIZATION

INTERNATIONAL CENTRE FOR SCIENCE AND HIGH TECHNOLOGY
c/o INTERNATIONAL CENTRE FOR THEORETICAL PHYSICS 34100 TRIESTE (ITALY) VIA GRIGNANO, 9 (ADRIATICO PALACE) P.O. BOX 586 TELEPHONE (040-224575) TELEFAX (040-224575) TELEX 460449 APH I

H4.SMR/540-27

Second Training College on Physics and Technology of Lasers and Optical Fibres

21 January - 15 February 1991

Switching and Modulation

A. Neyer
Universität Dortmund
Lehrstuhl für Hochfrequenztechnik
Dortmund, Germany

SWITCHING AND MODULATION

ANDREAS NEYER

UNIVERSITÄT DORTMUND, LEHRSTUHL FÜR
HOCHFREQUENZTECHNIK
4600 DORTMUND 50

(dipole moment per unit volume) is called polarisation **P** which is related to the driving electrical field **E** inside the material by

$$\mathbf{P} = \epsilon_0 \chi \mathbf{E} \qquad (1)$$

where ϵ_0=8.842 pF/m is the permittivity of vacuum and χ the dielectric susceptibility which is a scalar quantity in isotropic media. **P** has the dimension of a surface charge density. The result of the superposition of the internal electrical field of the optical radiation and that of the induced polarization is described by the dielectric displacement **D**. Like **P**, **D** has the dimension of a surface charge density.

$$\mathbf{D} = \epsilon_0 \mathbf{E} + \mathbf{P} = \epsilon_0 \epsilon \mathbf{E} \qquad (2)$$

ϵ is the relative dielectric constant which is related to the susceptibility by

$$\epsilon = \chi + 1 \qquad (3)$$

In an anisotropic medium the dielectric constant and the susceptibility are second-rank tensors with components ϵ_{ij} and χ_{ij}. The components of **D** and **P** along the coordinates x_1, x_2, and x_3 are given by

$$D_i = \epsilon_0 \epsilon_{ij} E_j \qquad (4)$$

$$P_i = \epsilon_0 (\epsilon_{ij} - 1) E_j = \epsilon_0 \chi_{ij} E_j \qquad (5)$$

It will always be understood in what follows that each term is to be summed over all repeated indices j = 1,2,3 (Einstein sum convention). Thus, (4) and (5) consist of three equations, the first of which is, e.g.

$$D_1 = \epsilon_0 (\epsilon_{11} E_1 + \epsilon_{12} E_2 + \epsilon_{13} E_3) \qquad (6)$$

As already mentioned, the interaction of the light with the bond charges of the medium will lead to a retardation of the light propagation. The resulting decrease in phase velocity v_p compared to the velocity of light in vacuum c_0 is generally expressed by the refractive index n

$$v_p / c_0 = 1/n \qquad (7)$$

Since the energy and therefore the frequency of the light must not depend on the actual medium (energy conservation), the wavelength of the lightwave in the medium is decreased as well by the factor 1/n: $\lambda_n = \lambda_0/n$ (see Fig.1). In isotropic and nonmagnetic media the refractive index is related to the relative dielectric constant ϵ by

$$n = \sqrt{\epsilon} \qquad (8)$$

Thus it is the refractive index which links the is the macroscopic observable phase retardation of an optical wave with the microscopic world of induced dipol moments due to the interaction of light with the medium. The refractive index is the fundamental quantity for characterizing the optical properties of a material.

In lossy media the refractive index is expressed by a complex number

$$\bar{n} = n + i\kappa \qquad (9)$$

where the real part (n) is responsible for the phase constant (phase retardation per unit length) and the imaginary part (κ) for the absorption. Both, the real and imaginary parts are not independent, but related by the Kramer's Kronig relation.

Since the refractive index of a medium contains all essential information about its interaction with light, the manipulation of light for modulation and switching implies a change of the refractive index. It will be shown that this is possible e.g. by strong electrical fields (electrooptic effect) or by mechanical strain fields which may be caused by acoustic waves (acoustooptic effect).

Frequently, the change of the refractive index of a medium as a function of electrical or strain fields is expressed by the change of the optical dielectric impermeability tensor η_{ij}

$$\eta_{ij} = 1/\epsilon_{ij} \qquad (10)$$

The components of the impermeability tensor along the principal axes of a crystal are $1/n_x^2$, $1/n_y^2$, $1/n_z^2$. In order to evaluate the consequences of electrooptic or acoustooptic changes of the impermeability tensor for the light propagation in anisotropic media, commonly the so called "index ellipsoid" (Fig.2) is used. It describes the energy density of the electrical field in the medium and is defined in the principal axes system by

$$x^2/n_x^2 + y^2/n_y^2 + z^2/n_z^2 = 1 \qquad (11)$$

where the main axes of the ellipsoid of lenghts $2n_x$, $2n_y$, $2n_z$ are parallel to the

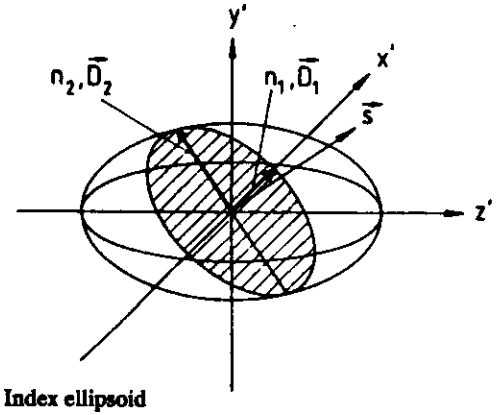

Fig. 2) Index ellipsoid

crystal axes. The index ellipsoid is a graphical construction which helps to find the indices of refraction for the two othogonally polarized light waves (D_1 and D_2) propagating through the crystal in the direction of the wavevector s which is normal to $D = D_1 + D_2$. The corresponding refractive indices n_1 and n_2 along the axes D_1 and D_2 are found from the length B_i of the semiprincipal axes of the elliptical intersection with the surface of the index ellipsoid by $n_i = 1/\sqrt{B_i}$. In certain types of crystals, the application of an electrical field results in a change in both the dimensions and the orientation of the index ellipsoid.

In addition to the already mentioned electrooptic and acoustooptic effects for changing the refractive index of a material, lossy media, especially semiconductors, offer the potential of an electrical control of the absorption coefficient. This may be utilized for the direct modulation of light (electroabsorption) or, indirectly, by changing the real part of n via the Kramers-Kronig relationship (electrorefraction).

III. PHYSICAL EFFECTS AND BASIC DEVICES FOR THE MODULATION AND SWITCHING OF LIGHT

A. ELECTROOPTICS

In this chapter we consider the modulation of light by the interaction with electrooptic crystals. Electrooptic crystals are characterized by the fact that they exhibit changes of their refractive indices in the presence of electrical fields. After a description of the electrooptic effect, basic electrooptic modulation schemes are reported.

1. The electrooptic effect

The propagation of optical radiation in a crystal can be described completely in terms of the impermeability tensor η_{ij} (10). According to the quantum theory of solids, this tensor depends on the distribution of charges in the crystal. The application of an electrical field will result in a redistribution of the bond charges and possibly in a slight deformation of the ion lattice. The net result is a change in the optical impermeability tensor. This is known as the electro-optic effect. The electro-optic coefficients are defined traditionally as

$$\eta_{ij}(E^{el}) - \eta_{ij}(0) = \Delta\eta_{ij} = r_{ijk} E_k^{el} + s_{ijkl} E_k^{el} E_l^{el} \qquad (12)$$

where E^{el} is the applied electrical field. The constants r_{ijk} and s_{ijkl} are the linear (or Pockels) and quadratic (or Kerr) electrooptic coefficients.

Thus the index ellipsoid of a crystal (11) in the presence of an applied electrical field may be written as

$$\eta_{ij}(E)\, x_i x_j = 1 \qquad (13)$$

It can be shown from the requirement of energy conservation that the dielectric tensor ϵ_{ij} and, in consequence, as well the impermeability tensor η_{ij}, are symmetric and that, therefore, the indices i and j can be permuted. Because of this permutation symmetry, it is convenient to introduce contracted indices to abreviate the notation. The contracted indices are defined as

$$1 = (11);\ 2 = (22);\ 3 = (33);$$
$$4 = (23) = (32);\ 5 = (13) = (31);\ 6 = (12) = (21) \qquad (14)$$

with 1 = x, 2 = y, and 3 = z.

The permutation symmetry reduces the number of independent elements of r_{ijk} from 27 to 18 and of s_{ijkl} from 81 to 36.

In the following, only the linear electrooptic effect will be considered, since the quadratic effect may be neglected if the linear effect is present. However, the linear electrooptic effect will be nonzero only in crystals with no inversion centre. This statement becomes clear, if we realize that the 'linear electrooptic effect' is in fact a 'nonlinear optical effect', that is, a consequence of the nonlinear response of the induced polarization P as a function of the driving elecrical field E. Treating P and E for this explanation as scalar quantities, we may express P as a Taylor expansion in terms of powers of E:

$$P = \sum_n \epsilon_0 \chi^{(n)} E^n \qquad (15)$$

where $\chi^{(n)}$ is the coefficient associated with the n-th power of E. Here, $\chi^{(1)}$ is the linear susceptibility and $\chi^{(2)}$ gives the first nonlinear term which is related to the linear electrooptic coefficient (in tensor notation) by

$$\chi_{ijk}^{(2)} = r_{ijk}\, \epsilon_{ii}\, \epsilon_{jj} \qquad (16)$$

Now, inversion symmetry (about the origin of the coordinates of the atoms making up the medium) requires that P will reverse its sign, if E is reversed: P (-E) = - P (E). This is the definition of an odd function which implies that P(E) must have no even terms and that, therefore, all $\chi^{(2m)}$ coefficients with m integer must vanish.

Assuming a crystal structure with no inversion symmetry and using the contracted indices (14), the equation of the index ellipsoid in the presence of an electrical field can be written

$$(1/n_x^2 + r_{1k} E_k)\, x^2 + (1/n_y^2 + r_{2k} E_k)\, y^2 + (1/n_z^2 + r_{3k} E_k)\, z^2$$
$$2\, y\, z\, r_{4k} E_k + 2\, z\, x\, r_{5k} E_k + 2\, x\, y\, r_{6k} E_k = 0 \qquad (17)$$

where E_k is the component of the applied electrical field and summation over repeated indices k is assumed. Here 1, 2, and 3 correspond to the principal dielectric axes x, y, z, and n_x, n_y, n_z are the principal refractive indices. In general, the principal axes of the ellipsoid (17) do not coincide with the unperturbed axes (x, y, z). A new set of principal axes (x', y', z') can always be found by a coordinate rotation, which is known as principal-axis transformation. The dimensions and orientation of the ellipsoid are, of course, dependent on the direction of the applied field as well as on the 18 matrix elements r_{lk}.

2. Basic electrooptic devices

Example 1: Electrooptic phase modulator in $LiNbO_3$

$LiNbO_3$ is a birefringent crystal with the two refractive indices n_o (ordinary index) and n_e (extraordinary index) for light polarized perpendicular or parallel to the optical axis, respectively. The crystal belongs to the symmetry group 3m and has eight nonvanishing electrooptic coefficients (r_{51}, r_{61}, r_{12}, r_{22}, r_{42}, r_{13}, r_{23}, r_{33}) four of which are independent: $r_{51} = r_{42}$; $r_{22} = -r_{61} = -r_{12}$; $r_{13} = r_{23}$ and r_{33}. We now consider the case when the electrical field is applied along the optical axis (z) of the crystal (Fig.3). Then the equation of the index ellipsoid can be written, according to (17), as

$$(1/n_o^2 + r_{13} E_z)\, x^2 + (1/n_o^2 + r_{13} E_z)\, y^2 + (1/n_e^2 + r_{33} E_z)\, z^2 = 0 \qquad (18)$$

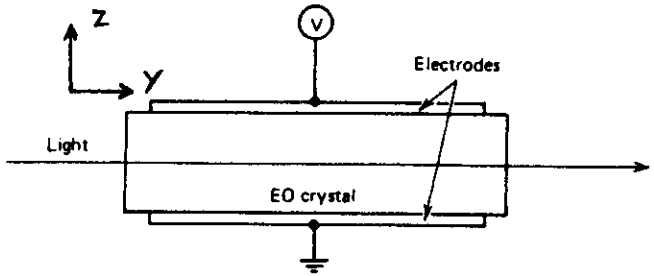

Fig. 3) Geometry of a transverse electro-optic modulator.

Since no mixed terms appear in (18), the principal axes of the new ellipsoid remain unchanged. The lengths of the new semiaxes are

$$n_x = n_o - 1/2\, n_o^3\, r_{13}\, E_z \qquad (19)$$

$$n_y = n_o - 1/2\, n_o^3\, r_{13}\, E_z \qquad (20)$$

$$n_z = n_e - 1/2\, n_e^3\, r_{33}\, E_z \qquad (21)$$

where the approximation

$$(1 + x)^{-1/2} \approx 1 - 1/2\, x \qquad (22)$$

has been utilized for $x \ll 1$. From (21) we see, for example, that a light wave polarized along the optical axis (z) will experience an electrooptical induced index change of

$$\Delta n_e = - 1/2\, n_e^3\, r_{33}\, E_z \qquad (23)$$

which will lead after the propagation along a distance L to a phase retardation of

$$\Delta\varphi = k\, \Delta n_e\, L = \pi/\lambda\, n_e^3\, r_{33}\, E_z\, L \qquad (24)$$

where k and λ are the wavenumber and wavelength of the light in vacuum, respectively. Since r_{33} is the strongest electrooptic coefficient in $LiNbO_3$, (24) may be utilized to built up efficient electrooptic phase modulators.

Example 2: Electrooptic intensity modulation by elctrooptically controlled birefringence

Gallium Arsenide and Indium Phosphite are examples for cubic crystals of the symmetry group 4 3 m. Without applied electrical fields these materials are optically isotropic and have the refractive index n along all three crystal axes. The only non vanishing electrooptic coefficients are r_{41}, r_{52}, and r_{63} which have identical values. Assuming an applied electrical field in the [0,1,1] direction of the crystal $E^{el} = E/\sqrt{2}(0, 1, 1)$, the resulting index ellipsoid gets the form

$$1/n^2 (x^2 + y^2 + z^2) + \sqrt{2} E r_{41} x z + \sqrt{2} E r_{41} x y = 1 \qquad (25)$$

We thus find that the application of an electrical field causes the appearance of "mixed" terms (xz, xy). This means that the major axes of the ellipsoid, with a field applied, are no longer parallel to the x,y,and z crystal axes. However, it can be shown, that a rotation of the index ellipsoid by 45° in the xz- and xy-plane transforms (25) into a new index ellipsoid with the main axes parallel to the transformed coordinate system x', y', z' (Fig.4). The semiaxes of the transformed index ellipsoid are given by

$$n_{x'} = n + n^3 r_{41} E/2 \qquad (26)$$

$$n_{y'} = n - n^3 r_{41} E/2 \qquad (27)$$

$$n_{z'} = n \qquad (28)$$

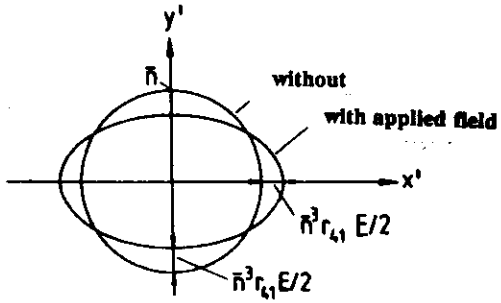

Fig. 4)

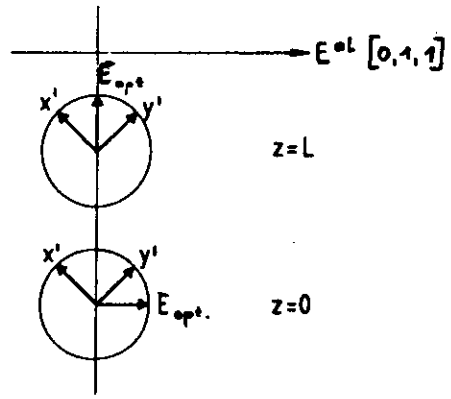

Fig. 5)

If we now consider a light wave linearly polarized along the (-1,1) direction in the new (') coordinate system propagating in z' - direction (Fig.5), the wave can be decomposed in a component parallel to x' and one parallel to y'. These two components will suffer different phase retardations after the propagation along a distance L

$$\Delta\varphi_{x'} = k \Delta n(E) L \qquad (29)$$

$$\Delta\varphi_{y'} = - k \Delta n(E) L \qquad (30)$$

where k is the vacuum wavenumber $2\pi/\lambda$ and $\Delta n(E)$ the electrooptic index change given by (27) and (28). Increasing the electrical field up to the point that the phase difference between the two orthogonal optical components reaches π,

$$\Delta\varphi(E_\pi) = \Delta\varphi_{x'} - \Delta\varphi_{y'} = 2\pi/\lambda\, n^3 r_{41} L E_\pi = \pi \qquad (31)$$

the resulting optical field vector will be rotated by 90° beeing polarized now along the (1,1) direction. This ectrooptically induced rotation of the optical field vector may be transformed into an intensity modulation, if a linear polarizer is placed behind the electrooptic crystal. The transmission through the polarizer may be written as

$$T = P_{out} / P_{in} = \cos^2(\pi E_z / 2 E_\pi) \qquad (32)$$

Substituting E_z by U/d, where U is the applied voltage and d the separation between the electrodes, and substituting E_π by U_π/d, we get the usually found expression for the sinusoidal transmission characteristic of electrooptic modulators which involve the interference between two optical waves

$$T(U) = \cos^2(\pi U / 2U_\pi) = 1/2\,(1 + \cos(\pi U / U_\pi)) \qquad (33)$$

The voltage required to switch from full to zero transmission is the so called 'half-wave voltage' U_π which results from (31) for cubic crystals as

$$U_\pi = d/L\ \lambda/2n^3 r_{41} \qquad (34)$$

The described modulator belongs to the class of transverse electrooptic modulators which means that the applied electrical field is transverse to the optical beam path. The main advantage of this configuration is that the modulation voltage may be reduced by increasing the length L. Besides further cubic crystals like InP, CuCl, and CdTe, ferroelectric crystals of the symmetry group 3m like $LiNbO_3$ and $LiTaO_3$ are used as transverse electrooptic modulators (see Fig.3). The half-wave voltage for $LiNbO_3$ and $LiTaO_3$ intensity modulators is given by

$$U_\pi = d/L\ \lambda/(n_e^3 r_{33} - n_o^3 r_{13}) \qquad (35)$$

The second class of electrooptic modulators are of the longitudinal type, where the electrical field is parallel to the optical beam path of the light. Examples are z-cut (light propagation along the optical z axis) KDP and $LiNbO_3$ and z-cut cubic crystals (GaAs, InAs, CdTe, ZnS). The $LiNbO_3$ longitudinal modulator is only suited for phase modulation, since there is no electrooptic change of the birefringence in this configuration. The U_π voltage required for a phase retardation of π is given by

$$U_\pi = \lambda / n_o^3 r_{13} \qquad (36)$$

KDP as well as the cubic crystals show even in this longitudinal geometry an electrooptic control of the birefringence. Therefore they may be used for amplitude modulation. The half-wave voltages are for KDP

$$U_\pi = \lambda / 2 n_o^3 r_{63} \qquad (37)$$

and for the cubic crystals

$$U_\pi = \lambda / 2 n^3 r_{41} \qquad (38)$$

These half-wave voltages are independent of the length of the crystal, proportional to the wavelength and inverse proportional to the electrooptic coefficients. These voltages at visible wavelenghts are of the order of several kilovolts. The need to use high voltages becomes very serious for infrared radiation because of the long wavelenth of the light (e.g. 10.6 μm). Longitudinal modulators are used only when large acceptance area and wide field of view are required.

Copy from R.G.Hunsperger, "Integrated Optics: Theory and technology", Springer Series in Optical Sciences, Vol. 33, Springer 1985, pp 120

8.1 Basic Operating Characteristics of Switches and Modulators

8.1.1 Modulation Depth

One important characteristic of modulators and switches is the modulation depth, or modulation index, η. In the case of an intensity modulator in which the applied electrical signal acts to decrease the intensity of the transmitted light, η is given by

$$\eta = (I_0 - I)/I_0\,, \qquad (8.1.1)$$

where I is the transmitted intensity and I_0 is the value of I with no electrical signal applied. If the applied electrical signal acts to increase the transmitted light intensity, η is given by

$$\eta = (I - I_0)/I_m\,, \qquad (8.1.2)$$

where I_m is the transmitted intensity when maximum signal is applied. The maximum modulation depth, or extinction ratio, is given by

$$\eta_{max} = (I_0 - I_m)/I_0 \quad \text{for} \quad I_m \leqq I_0\,. \qquad (8.1.3)$$

or by

$$\eta_{max} = (I_m - I_0)\, I_m \quad \text{for} \quad I_m \geqq I_0\,. \qquad (8.1.4)$$

It is also possible to define the modulation depth for phase modulators, as long as the phase change can be functionally related to an equivalent intensity change. For the case of interference modulators, it can be shown that the modulation depth is given by [8.1, 2]

$$\eta = \sin^2(\Delta\varphi/2)\,, \qquad (8.1.5)$$

where $\Delta\varphi$ is the phase change.

Modulation depth has been defined for intensity modulators (and indirectly for phase modulators); however, an analogous figure of merit, the maximum deviation of a frequency modulator, is given by

$$D_{max} = |f_m - f_0|/f_0\,, \qquad (8.1.6)$$

where f_0 is the optical carrier frequency, and f_m is the shifted optical frequency when the maximum electrical signal is applied.

8.1.2 Bandwidth

Another important characteristic of modulators and switches is the bandwidth, or range of modulation frequencies over which the device can be operated. By convention, that bandwidth of a modulator is usually taken as the difference between the upper and lower frequencies at which the modulation depth falls to 50% of its maximum value. In the case of a switch, frequency response is usually given in terms of the switching speed, or switching time. The switching time T is related to the bandwidth Δf by the expression

$$T = 2\pi/\Delta f. \tag{8.1.7}$$

Minimizing switching time is most important when large-scale arrays of switches are used to route optical waves over desired paths. Similarly, modulation bandwidth is a critical factor when many information channels are to be multiplexed onto the same optical beam. Thus, the unusually fast switching speed and wide bandwidth of waveguide switches and modulators, which will be discussed later in this chapter, make them particularly useful in large telecommunications systems.

8.1.3 Insertion Loss

Insertion loss is another important characteristic of optical switches and modulators that must be known for system design. Insertion loss is generally stated in decibels, and for the case in which the modulating signal acts to decrease the intensity, it is given by

$$\mathcal{L}_i = 10 \log (I_t/I_0), \tag{8.1.8}$$

where I_t is the optical intensity that would be transmitted by the waveguide if the modulator were absent, and I_0 is the intensity transmitted with the modulator in place, but with no applied signal. For a modulator in which the applied signal acts to increase the transmitted intensity, the insertion loss is given by

$$\mathcal{L}_i = 10 \log (I_t/I_m), \tag{8.1.9}$$

where I_m is the transmitted intensity when maximum signal is applied. Insertion loss is, of course, an optical power loss. However, it ultimately increases the amount of electrical power that must be supplied to the system, since higher power optical sources must be used.

8.1.4 Power Consumption

Electrical power must also be supplied to drive the modulator or switch. In the case of modulators, the required drive power increases with modulation frequency. Hence, a useful figure of merit is the drive power per unit bandwidth, $P/\Delta f$, usually expressed in milliwatts per megahertz. As is discussed in more detail in Sect. 8.7, a key advantage of channel-waveguide modulators is that they have a significantly lower $P/\Delta f$ than that required for bulk modulators.

The power requirements of optical switches operating at high clock rates, for example to time-division multiplex a number of different signals, can be evaluated in much the same way as is used for modulators. Hence, $P/\Delta f$ would still be a useful figure of merit in that case. However, if switching is done at relatively slow rates, a more important quantity is the amount of power required to hold the switch in a given state. An ideal switch would consume significant power only during the change of state; holding power would be negligible. Since electro-optic switches require the presence of an electric field to maintain at least one state, they could not be called ideal in that respect. However, except for leakage current, little power is needed to maintain a field in the small volume of a waveguide switch.

8.1.5 Isolation

The degree of isolation between various inputs and outputs of a switch or modulator is a major design consideration. In a modulator, the isolation between input and output is merely the maximum modulation index, as defined previously. However, it is usually expressed in decibels when used to specify isolation. In the case of a switch, the isolation between two ports (either input or output) is given by

$$\text{isolation [dB]} = 10 \log \frac{I_2}{I_1}, \tag{8.1.10}$$

where I_1 is the optical intensity in the driving port, and I_2 is the intensity at the driven port when the switch is in the *off* state with respect to port 1 and 2. Thus, a switch with a signal leakage, or crosstalk, of 1% with respect to two ports would have – 20 dB isolation.

8.3. SOME DESIGN CONSIDERATIONS *

8.3.1. High-Frequency Modulation Considerations

In this section we consider some of the basic factors limiting the highest usable modulation frequencies in a number of typical experimental situations.

Consider first the situation described by Fig. 8.9. The electro-optic crystal is placed between two electrodes with a modulation field containing frequencies near $\omega_0/2\pi$ applied to them. R_s is the internal resistance of the modulation source, and C represents the parallel-plate capacitance due to the electro-optic crystal. If $R_s > (\omega_0 C)^{-1}$, most of the modulation voltage drop is across R_s and is thus wasted, since it does not contribute to the retardation. This can be remedied by resonating the crystal capacitance with an inductance L, where $\omega_0^2 = (LC)^{-1}$, as shown in Fig. 8.9. In addition, a

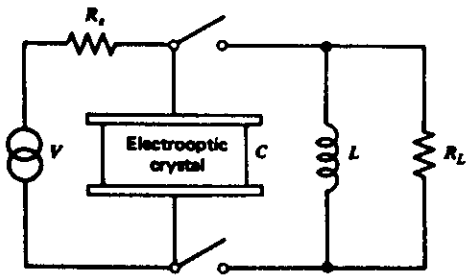

Figure 8.9. Equivalent circuit of an electro-optic modulation crystal in a parallel-plate configuration.

shunting resistance R_L is used so that at $\omega = \omega_0$ the impedance of the parallel RLC circuit is R_L, which is chosen to be larger than R_s, so most of the modulation voltage appears across the crystal. The resonant circuit has a finite bandwidth—that is, its impedance is high only over a frequency interval $\Delta\omega/2\pi \approx 1/(2\pi R_L C)$ (centered on ω_0). Therefore, the maximum modulation bandwidth (the frequency spectrum occupied by the modulation signal) must be less than

$$\frac{\Delta\omega}{2\pi} \approx \frac{1}{2\pi R_L C} \tag{8.3-1}$$

if the modulation field is to be a faithful replica of the modulation signal.

* Copy from A. Yariv, P.Yeh, "Optical Waves in Crystals", John Wiley, New York

8.3.2. Transit-Time Limitations in a Lumped Modulator

Another important high-frequency modulation consideration is the transit-time limitations in a lumped modulator. In the event that the modulating

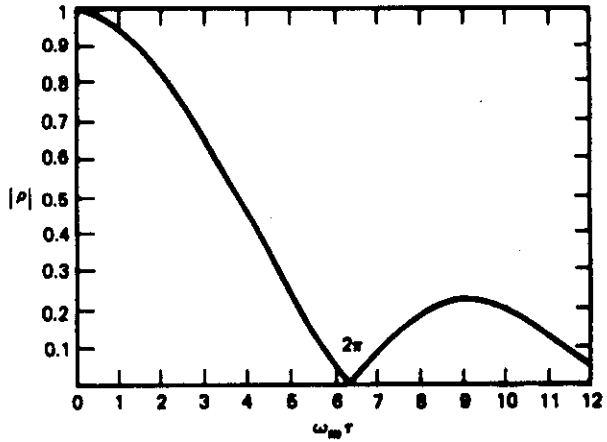

Figure 8.10. Magnitude of the transit-time reduction factor ρ versus $\omega_m t$.

field is a very fast-varying function of time, the optical phase no longer follows the time-varying refractive index adiabatically, especially when the transit time $\tau = nL/c$ is comparable to the period $2\pi/\omega_m$ of the modulating field.

$$\rho = \frac{\sin\frac{1}{2}\omega_m\tau}{\frac{1}{2}\omega_m\tau}, \tag{8.3-3}$$

where ω_m is the modulation frequency.

For $\rho \approx 1$ (i.e., no reduction), the condition $\omega_m\tau \ll 1$ must be satisfied, that is, the transit time must be small compared to the shortest modulation period. The factor ρ is plotted in Fig. 8.10.

If, somewhat arbitrarily, we take the highest useful modulation frequency as that for which $\omega_m\tau = \pi$ (at this point, according to Fig. 8.10, $\rho = 0.64$), and we use the relation $\tau = Ln/c$, we obtain

$$(\nu_m)_{max} = \frac{c}{2Ln}, \tag{8.3-4}$$

which using a KDP crystal ($n \simeq 1.5$) and a length $L = 2$ cm, yields $(\nu_m)_{max} = 5 \times 10^9$ Hz.

8.3.3. Traveling-Wave Modulators

One method that can, in principle, overcome the transit-time limitation involves applying the modulation signal in the form of a traveling wave as shown in Fig. 8.11. It has been shown in Section 7.4 that if the optical- and modulation-field phase velocities are equal, a portion of an optical wavefront will experience the same instantaneous modulating electric field, which corresponds to the field it encounters at the entrance face, as it propagates through the crystal, and the transit-time problem discussed above is eliminated. This form of modulation is used mostly in the transverse geometry as discussed in the preceding section, since the RF field in most propagating structures is predominantly transverse.

In general, if there is a phase-velocity mismatch between the modulating wave and the light wave, a reduction factor in the modulation depth is given by Eq. (7.4-23). The maximum useful modulation frequency is taken, as in the treatment leading to Eq. (8.3-4), to be

$$(\nu_m)_{max} = \frac{c}{2L(n - n_m)}, \tag{8.3-5}$$

which, upon comparison with Eq. (8.3-4), shows an increase in the frequency limit or useful crystal length of $(1 - n_m/n)^{-1}$. We recall that n is the index of refraction of the medium at the frequency of the light beam and n_m is the index of refraction at the modulating frequency.

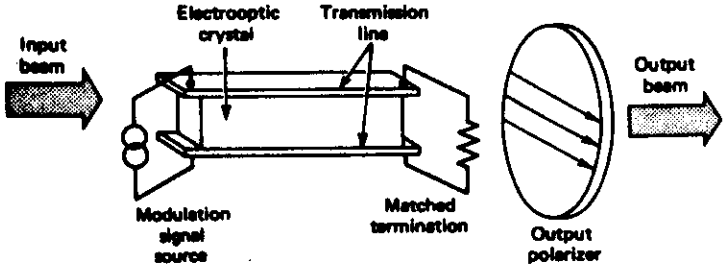

Figure 8.11. A traveling-wave electro-optic modulator.

8.3.4. Geometrical Considerations

In the discussion of the transverse electro-optic modulator, we found that in order to decrease the modulation voltage it is desirable to use a long crystal rod with small transverse dimension (i.e., large L/d). On the other hand, the transverse dimension d must be large enough to accommodate the light beam to be modulated. A light beam with a finite cross section will, in general, diverge as it propagates. Therefore, a crystal rod with a given transverse dimension d has a maximum useful length for electro-optic modulation.

Consider a Gaussian laser beam propagating in the lowest-order transverse mode and passing through an electro-optic crystal rod of length L and diameter d. Given a rod with a fixed length L, it can be shown that the diameter of the cylinder will be a minimum when the Gaussian beam is focused in such a way that the confocal parameter z_0 equals one-half the length L, and the beam waist is located at the center of the rod. This is illustrated in Fig. 8.12. Under these conditions, the beam diameter is $2\omega_0$ at the waist and $\sqrt{8}\,\omega_0$ at the input and output plane of the cylinder, where

$$\omega_0^2 = \frac{\lambda L}{2\pi n}, \tag{8.3-6}$$

and ω_0 is called the beam spot size. In practice, the diameter d is chosen to be larger than $\sqrt{8}\,\omega_0$ for ease of alignment. In Chapter IV we will discuss a guided-wave electro-optic modulator in which the light is

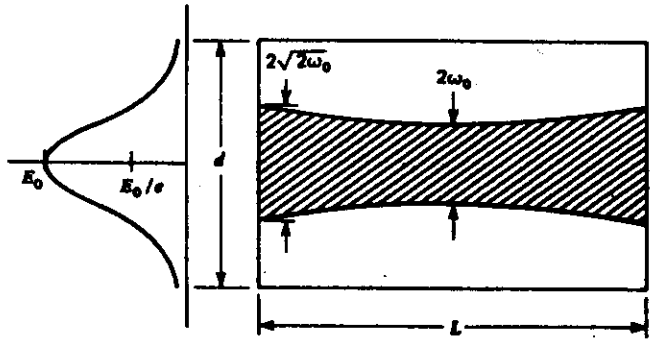

Figure 8.12. A beam of Gaussian cross section passing through a rod of diameter d and length L.

confined to a region with very small ($\sim \lambda$) transverse dimensions. Since the light is in a guided mode, there is no diffraction and the interaction path can be made very long.

B. ACOUSTOOPTICS ✱

Acoustooptics deals with the interaction of optical waves with the acoustic waves in material media. The most interesting phenomenon associated with the interaction of light with sound waves is the diffraction of light by the acoustically perturbed medium. When an acoustic wave propagates in a medium, there is an associated strain field. The strain results in a change in the index of refraction. This is referred to as the photoelstic effect. The strain field is a periodic function of position for a plane acoustic wave. Therefore, the index of refraction becomes periodically perturbed, as well, and Bragg coupling may take place. The manipulation of light by acousto-optic interaction is used in a number of applications, including light modulators, beam deflectors, signal processors, tunable filters, and spectrum analyzers.

9.1. THE PHOTOELASTIC EFFECT

The photoelastic effect in a material couples the mechanical strain to the optical index of refraction. This effect occurs in all states of matter and is traditionally described by

$$\Delta\eta_{ij} = \Delta\left(\frac{1}{n^2}\right)_{ij} = p_{ijkl}S_{kl}, \tag{9.1-1}$$

where $\Delta\eta_{ij}$ [or $\Delta(1/n^2)_{ij}$] is the change in the optical impermeability tensor and S_{kl} is the strain tensor. The coefficients p_{ijkl} form the strain–optic tensor. In the expression (9.1-1), higher-order terms involving powers of S_{kl} are neglected, because these terms are usually small compared with the linear term ($S_{kl} \sim 10^{-5}$ typically). The index ellipsoid of a crystal in the presence of an applied strain field is thus given by

$$(\eta_{ij} + p_{ijkl}S_{kl})x_i x_j = 1. \tag{9.1-2}$$

✱ Copy from A. Yariv, P.Yeh, "Optical Waves in Crystals", John Wiley, New York, 1984

Since both η_{ij} and S_{kl} are symmetric tensors, the indices i and j as well as k and l in Eq. (9.1-1) can be permuted. The permutation symmetry of the strain–optic tensor, p_{ijkl}, is identical to that of the quadratic electro-optic tensor s_{ijkl}, (7.2-9) and (7.1-8). It is thus convenient to use the contracted indices to abbreviate the notation. Equation (9.1-1) then becomes

$$\Delta\left(\frac{1}{n^2}\right)_i = p_{ij}S_j, \qquad i, j = 1, 2, \ldots, 6, \tag{9.1-3}$$

where S_j are the strain components. The strain–optic coefficients p_{ij} are usually defined in the principal coordinate system. The new index ellipsoid in the presence of the strain field is in general different from the zero-field index ellipsoid. The strain field changes the dimensions as well as the orientation of the index ellipsoid (7.1-1). This change is, of course, dependent upon the applied strain field as well as the strain–optic coefficients p_{ij} according to Eq. (9.1-4). The form, but not the magnitude, of the strain–optic coefficients p_{ij} can be derived from the symmetry of the crystal. This point-group symmetry dictates which of the 36 coefficients are zero, as well as relationships that may exist between the nonvanishing coefficients.

9.1.1. Example: The Acousto-optic Effect in Water

Consider the propagation of a sound wave in water. Let the sound wave be a longitudinal wave propagating along the z direction with the particle displacement given by

$$u(z, t) = A\hat{z}\cos(\Omega t - Kz),$$

where A is the amplitude of oscillation, Ω is the sound frequency, and K is the wave number. The strain field associated with this sound wave is

$$S_3 = KA\sin(\Omega t - Kz) = S\sin(\Omega t - Kz),$$

where S is defined as KA. Water is an isotropic medium. Thus, according to Table 9.1 and Eq. (9.1-3), the change in the dielectric impermeability is

$$\Delta\eta_{11} = \Delta\left(\frac{1}{n^2}\right)_1 = p_{12}S\sin(\Omega t - Kz),$$

$$\Delta\eta_{22} = \Delta\left(\frac{1}{n^2}\right)_2 = p_{12}S\sin(\Omega t - Kz),$$

$$\Delta\eta_{33} = \Delta\left(\frac{1}{n^2}\right)_3 = p_{11}S\sin(\Omega t - Kz),$$

$$\Delta\eta_{ij} = 0 \quad \text{for} \quad i \neq j.$$

Table 9.1.

Isotropic (2)

$$\begin{pmatrix} p_{11} & p_{12} & p_{12} & 0 & 0 & 0 \\ p_{12} & p_{11} & p_{12} & 0 & 0 & 0 \\ p_{12} & p_{12} & p_{11} & 0 & 0 & 0 \\ 0 & 0 & 0 & \frac{1}{2}(p_{11} - p_{12}) & 0 & 0 \\ 0 & 0 & 0 & 0 & \frac{1}{2}(p_{11} - p_{12}) & 0 \\ 0 & 0 & 0 & 0 & 0 & \frac{1}{2}(p_{11} - p_{12}) \end{pmatrix}$$

The new index ellipsoid can now be written

$$x^2\left[\frac{1}{n^2} + p_{12}S\sin(\Omega t - Kz)\right] + y^2\left[\frac{1}{n^2} + p_{12}S\sin(\Omega t - Kz)\right]$$

$$+ z^2\left[\frac{1}{n^2} + p_{11}S\sin(\Omega t - Kz)\right] = 0.$$

Since no mixed terms are involved, the principal axes remain unchanged.

The new principal indices of refraction are thus given by

$$n_x = n - \tfrac{1}{2}n^3 p_{12}S\sin(\Omega t - Kz),$$

$$n_y = n - \tfrac{1}{2}n^3 p_{12}S\sin(\Omega t - Kz),$$

$$n_z = n - \tfrac{1}{2}n^3 p_{11}S\sin(\Omega t - Kz),$$

where p_{11}, p_{12} are the strain–optic coefficients and n is the index of refraction of water. We notice that in the presence of the sound wave, the water becomes a periodic medium which is equivalent to a volume grating

9.2. BASIC CONCEPTS OF ACOUSTO-OPTIC INTERACTIONS

We now consider the propagation of a monochromatic plane light wave in a medium in which an acoustic wave is excited and the optical impermeability is periodically modulated. As shown in the examples in Section 9.1, the acoustic wave causes a change in the index of refraction of the medium. The medium becomes periodic with a period equal to that of the acoustic wavelength. This periodic perturbation is a function of both space and time. If the acoustic wave is a traveling wave, so is the periodic perturbation, which moves at a velocity equal to the sound velocity (typically a few times 10^3 m/s). Since the velocity of sound is some five orders of magnitude smaller than that of light ($c = 3 \times 10^8$ m/s), the periodic perturbation caused by the sound wave is essentially stationary. The problem reduces to one of electromagnetic propagation in a periodic medium, which is discussed in Chapter 6. As an example to illustrate the acousto-optic interaction, we consider the propagation of a light beam in water. The sound wave induces a change in the refractive indices due to the strain–optic effect. Let z be the axis in the direction of propagation of the sound wave, and the yz coordinate plane be parallel to the plane of incidence. If the light beam is linearly polarized in the x direction (TE wave), the index of refraction for this mode is, according to the example in Section 9.1.1,

$$n_x = n - \tfrac{1}{2}n^3 p_{12}S\sin(\Omega t - Kz), \tag{9.2-1}$$

where $\Omega/K = v$. Figure 9.1 illustrates this sinusoidal variation of the index of refraction.

BRAGG REFLECTION

If the transverse dimension of the acoustic wave is infinite, the kinematic biundary condition requires that the reflected beam lie in the plane of incidence (yz plane) with an angle of reflection equal to the angle of incidence (see Fi. 9.2). Strong reflection occurs, if the condition for constructive interference is fullfilled, that means, if the optical path difference between the reflections from two equivalent planes in the sound beam (planes separated by the sound wavelength) is an integer multiple of the optical wavelength

$$2\,\Lambda\sin\theta = m\,\lambda/n \quad m = 1, 2, 3 \ldots \tag{9.2-4}$$

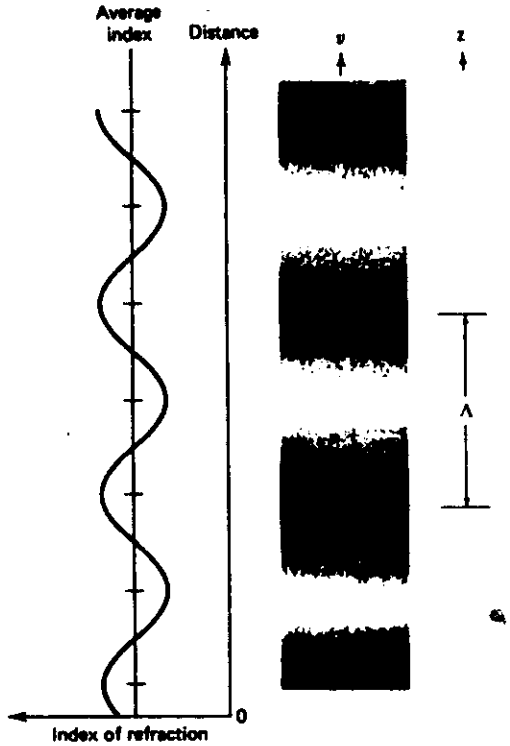

Figure 9.1. Traveling sound wave "frozen" at some instant of time. It consists of alternating regions of compression (dark) and rarefaction (white), which travel at the sound velocity v. Also shown is the instantaneous spatial variation of the index of refraction that accompanies the sound wave.

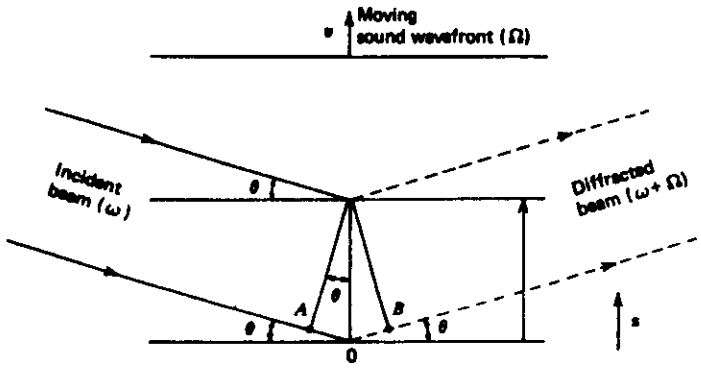

Figure 9.2. The reflections from two equivalent planes in the sound beam (that is, planes separated by the sound wavelength Λ), which add up in phase along the direction θ if the optical path difference $AO + OB$ is equal to one optical wavelength.

DOPPLER FREQUENCY SHIFT

The Bragg diffraction condition (9.2-4) is derived by assuming that the periodic perturbation is fixed relative to the light beam. The effect of the displacement can be derived by considering the Doppler shift undergone by an optical beam incident on a mirror moving at the sound velocity v at an angle satisfying the Bragg condition (9.2-4). The formula for the Doppler frequency shift of a wave reflected from a moving object is

$$\Delta\omega = 2\omega\frac{v_{\parallel}}{c/n},$$

where ω is the optical frequency and $v_{\parallel}$ is the projection of the object velocity vector along the wave propagation direction. From Fig. 9.2 we have $v_{\parallel} = v\sin\theta$, and thus

$$\Delta\omega = 2\omega\frac{v\sin\theta}{c/n}. \tag{9.2-5}$$

Using Eq. (9.2-4) for $\sin\theta$, we obtain

$$\Delta\omega = \frac{2\pi v}{\Lambda} = \Omega, \tag{9.2-6}$$

and therefore the frequency of the reflected light beam is upshifted by Ω.

If the direction of propagation of the sound beam is reversed so that, in Fig. 9.2, the sound recedes from the optical beam, the Doppler shift changes sign and the diffracted beam has a frequency $\omega - \Omega$.

10

Acousto-optic Devices *

The interaction of light beams with a sound wave in a photoelastic medium is shown in Chapter 9 to exhibit many interesting effects. These effects (e.g., Bragg diffraction) can be used to build light modulators, beam deflectors, tunable filters, spectral analyzers, and signal processors. The use of acousto-optic interactions offers the possibility of manipulating a laser beam or processing signal radiation at high speed, since no mechanical moving parts are involved. This property is very similar to that of the electro-optic modulation, except that in the acousto-optic interaction an RF field is required instead of a dc field. Recent advances in the acousto-optic device applications have resulted principally from the availability of lasers, which produce intense, coherent light beams; from the development of efficient broadband transducers which generate elastic waves up to microwave frequencies; and from the discovery of materials that have excellent elastic and optical properties. In this chapter we will study various device applications which utilize Bragg diffraction. The transmission characteristics, diffraction efficiencies, operation bandwidth, and other design considerations will be discussed.

10.1. ACOUSTO-OPTIC MODULATORS

The acousto-optic interaction can be used to construct a variety of light modulators. Both amplitude modulation and frequency translation can be achieved.

In this section, modulators operating in the Bragg regime ($2\pi\lambda L/n\Lambda^2 > 1$) will be emphasized, since only high-frequency modulators can give the very wide bandwidths which are of interest. From Eq. (9.5-29) it is seen that the fraction of light diffracted is

$$\eta = \frac{I_{\text{diffracted}}}{I_{\text{incident}}} = \sin^2\left(\frac{\pi L}{\lambda\sqrt{2}\cos\theta_B}\sqrt{MI_a}\right), \tag{10.1-1}$$

where L is the length of interaction, λ is the wavelength of light, θ_B is the Bragg angle, I_a is the acoustic intensity, and M is the figure of merit of the material.

* Copy from A. Yariv, P.Yeh, "Optical Waves in Crystals", John Wiley, New York, 1984

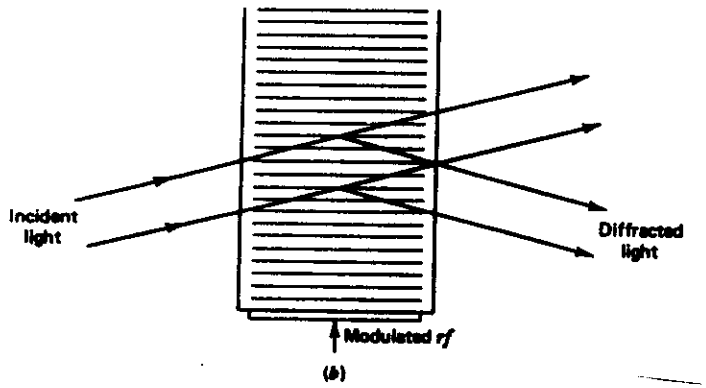

Figure 10.1. Acousto-optic light modulators: Bragg regime.

For small acoustic power levels, the diffraction efficiency η increases monotonically with the acoustic intensity:

$$\eta \simeq \frac{\pi^2 L^2}{2\lambda^2\cos^2\theta_B} MI_a. \tag{10.1-2}$$

Therefore, if the acoustic intensity is modulated, so is the diffracted light-beam intensity. Thus acousto-optic Bragg diffraction offers a way of imprinting information on the optical beam. The Bragg diffraction, of course, occurs with acceptable efficiency only when the directions of incident and diffracted light are approximately symmetrical with respect to the acoustic wavefronts. The angle of incidence and diffraction is then known as the Bragg angle θ_B and is given by

$$\theta_B = \sin^{-1}\frac{\lambda}{2n\Lambda} = \sin^{-1}\frac{\lambda f}{2nv}, \tag{10.1-3a}$$

where n is the index of refraction of the medium, v is the phase velocity of sound, and f is the sound frequency. In practice, the Bragg angle θ_B is small, so Eq. (10.1-3a) can be written as

$$\theta_B = \frac{\lambda}{2n\Lambda} = \frac{\lambda f}{2nv}. \tag{10.1-3b}$$

For small Bragg angle θ_B, the angle of deflection $2\theta_B$ is linearly proportional to the sound frequency. This is the basic principle of operation of an acousto-optic beam deflector

10.2. ACOUSTO-OPTIC DEFLECTORS

One of the most important applications of acousto-optic interactions is in the deflection of optical beams. Basically, acousto-optic deflectors operate in the same way as Bragg diffraction modulators, the only difference being that the frequency rather than the amplitude of the sound wave is varied. The use of acousto-optic interaction offers the possibility of high-resolution beam deflection. Both random-access and continuously scanned deflectors can be obtained. The basic principle of operation is depicted in Fig. 10.4

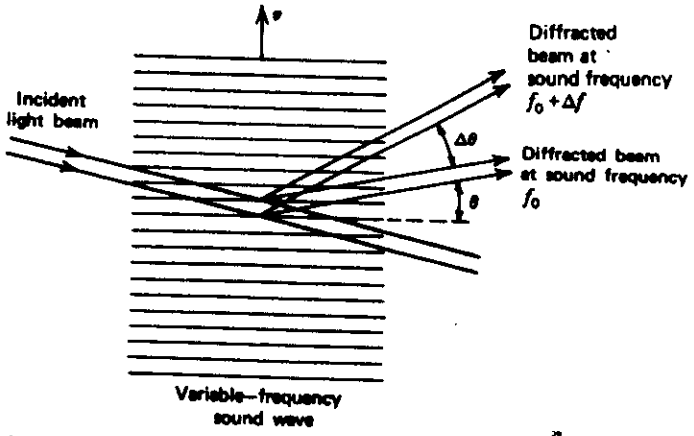

Figure 10.4. A change of frequency of the sound wave from f_0 to $f_0 + \Delta f$ causes a change $\Delta\theta$ in the direction of the diffracted beam, according to Eq. (10.2-1).

A common figure of merit for a deflector is the ratio of the total number of resolvable spots to the access time, expressed as a speed–capacity product, which, according to Eq. (10.2-2), is

$$\frac{N}{\tau} = \Delta f. \tag{10.2-3}$$

Thus, a high speed–capacity product is only available when the bandwidth Δf is large. It is therefore desirable to use high-frequency sound waves for beam deflectors, because large bandwidth Δf is only possible when the modulation frequency f_0 is high.

10.3. ACOUSTO-OPTIC TUNABLE FILTERS (AOTF)

Another important application of the acousto-optic interaction is in the construction of a spectral tunable filter. Normally, an acousto-optic tunable filter employs the large-angle codirectional acousto-optic interaction.

In codirectional coupling between the two waves, the diffracted (A_2) and the incident (A_1) waves are both propagating in the same direction [either both $+z$ or $-z$; see Fig. 9.8(a)].

These two waves which are frequently of orthogonal polarizations are coupled by an acoustic shear wave.

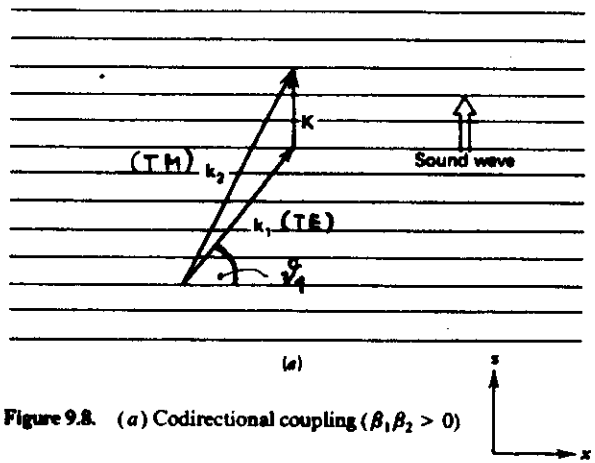

Figure 9.8. (a) Codirectional coupling ($\beta_1\beta_2 > 0$)

Strong acousto-optic interaction occurs only when the Bragg condition (conservation of momentum) is satisfied. If the incident light beam contains many spectral components, only one will satisfy the Bragg condition at a given acoustic frequency. In other words, only one spectral component will be diffracted at a given acoustic frequency. Therefore, by varying the acoustic frequency, the frequency (or wavelength) of the diffracted beam can also be varied. The fraction of power transferred from the incident beam to the diffracted beam in an interaction length L is given

by

$$T = \frac{\sin^2\left[\kappa_{12}L\sqrt{1 + (\Delta\beta/2\kappa_{12})^2}\right]}{1 + (\Delta\beta/2\kappa_{12})^2}, \tag{10.3-1}$$

where κ_{12} is the magnitude of the coupling constant (9.5-46), and $\Delta\beta$ is the momentum mismatch

$$\Delta\beta = \beta_1 - \beta_2 \pm K. \tag{10.3-2}$$

β_1 and β_2 are the components of the wave vectors of the incident and the diffracted beam, respectively, along the direction of propagation of the acoustic wave. Let θ_1 and θ_2 be the angles of the wave vectors measured from the wavefronts of the sound wave, such that

$$\begin{aligned} \beta_1 &= \frac{\omega}{c} n_1 \sin\theta_1 = \frac{2\pi}{\lambda} n_1 \sin\theta_1, \\ \beta_2 &= \frac{\omega}{c} n_2 \sin\theta_2 = \frac{2\pi}{\lambda} n_2 \sin\theta_2, \end{aligned} \tag{10.3-3}$$

where n_1 and n_2 are the refractive indices associated with the incident and diffracted waves, respectively. The conservation of momentum (Bragg condition) $\Delta\beta = 0$ becomes

$$\frac{2\pi}{\lambda}(n_2 \sin\theta_2 - n_1 \sin\theta_1) = \pm\frac{2\pi}{v} f, \tag{10.3-4}$$

where f is the acoustic frequency and v is the velocity of sound in the medium.

From Eq. (10.3-4) it is seen that the wave number $(2\pi/\lambda)$ of the diffracted light is proportional to the acoustic frequency f. An ideal acousto-optic tunable filter is normally operated at the condition when

$$\kappa_{12}L = \tfrac{1}{2}\pi, \tag{10.3-5}$$

so that the power conversion is 100% when the phase-matching condition $\Delta\beta = 0$ (10.3-4) is satisfied. Substituting Eq. (10.3-5) for κ_{12} in Eq. (10.3-1), the conversion efficiency (10.3-1) becomes

$$T = \frac{\sin^2\left[\frac{1}{2}\pi\sqrt{1 + (\Delta\beta L/\pi)^2}\right]}{1 + (\Delta\beta L/\pi)^2}. \tag{10.3-6}$$

Thus the conversion efficiency drops to 50% when

$$\Delta\beta L = \pm 0.80\pi, \tag{10.3-7}$$

where L is the interaction length of the optical and acoustic fields. This corresponds to a bandwidth (full width at half maximum), according to Eqs. (10.3-4) and (10.3-7), of

$$\Delta\lambda_{1/2} = \frac{0.80\lambda^2}{|n_2 \sin\theta_2 - n_1 \sin\theta_1|L} \tag{10.3-8}$$

which, for the collinear case ($\theta_1 = \theta_2 = \frac{1}{2}\pi$), reduces to

$$\Delta\lambda_{1/2} = \frac{0.80\lambda^2}{|\Delta n|L} \quad \text{(collinear interaction)}. \tag{10.3-9}$$

According to Eqs. (10.3-8) and (10.3-9), the bandpass width is inversely proportional to the interaction length L. The filter transmission T (or conversion efficiency) at a given acoustic frequency versus the normalized optical frequency deviation $\Delta\beta L$ is plotted in Fig. 10.11.

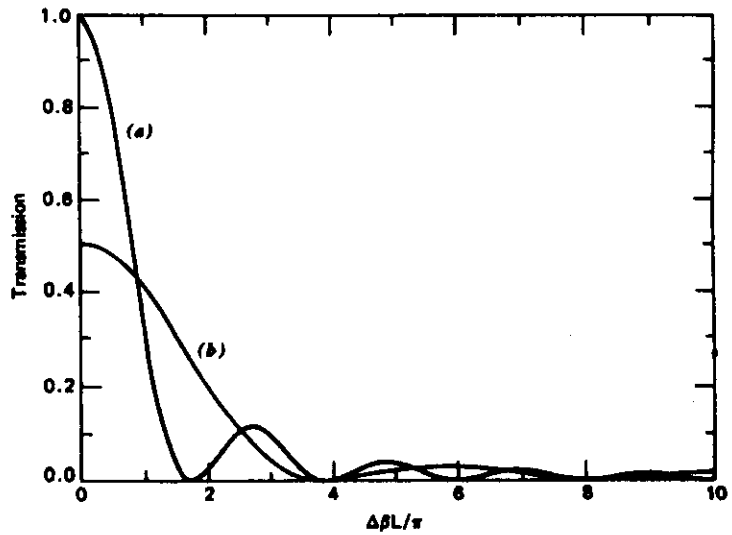

Figure 10.11. Calculated transmission of an acousto-optic tunable filter versus the normalized frequency deviation ($\Delta\beta L/\pi$): (a) peak transmission = 100% ($\alpha = 1$); (b) peak transmission = 50% ($\alpha = \frac{1}{2}$). The parameter α appears in Eq. (10.3-13).

C. ELECTROABSORPTION

Besides the electrooptic and acoustooptic effects, semiconductor materials allow the utilization of the electrical control of the absorption. The change of the fundamental absorption of semiconductors by applied electrical fields is called electroabsorption or Franz-Keldysh effect.

To understand this effect let us consider Fig. C1. In an homogeneous electrical field (along the x-direction) the edges of the valence and conduction bands are tilted. The separation between the band edges along x is d.

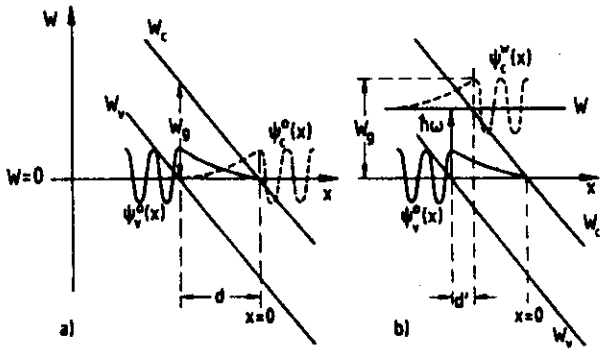

FIG. C1

From the overlapping wavefunctions of the valence and conduction electrons (and selection rules) there results a certain probability for the valence electron to get into the conduction band by tunneling. This tunneling process may be substantially enhanced by the absorption of a photon with energy $\hbar\omega$, since by the absorption of a photon the energy level of the electron in the conduction band will be increased by $W = \hbar\omega$. Because of the tilted band edges the effective separartion between valence and conduction band along the x-direction is reduced by this mean from d to d'

This reduction of the barrier width will enhance drastically the tunneling probalility of the electrons and therefore the absorption. Thus the electroabsorption may be understood as a photonabsorption enhanced tunneling effect in semiconductors under applied electrical fields.

D. ELECTROREFRACTION

As already mentioned in II. (9), the real and imaginary parts of the refractive index are not independent and are related via the Kramers-Kronig relation. Therefore, the change of the absorption (imaginary part of n) will result in a change of the real part of the refractive index. This is known as electrorefraction. The electrorefraction may be calculated, if the complete spectrum of the absorption is known.

Fig. D1 shows the calculated change of the refractive index as a function of the energy of the incident photons at different electrical field strengths. The achieved index changes in the order of some 10^{-3} are quite considerable, but they are hardly to be utilized for e.g. phase modulation, since at the relevant electrical field strenghts the devices will show rather strong absorption.

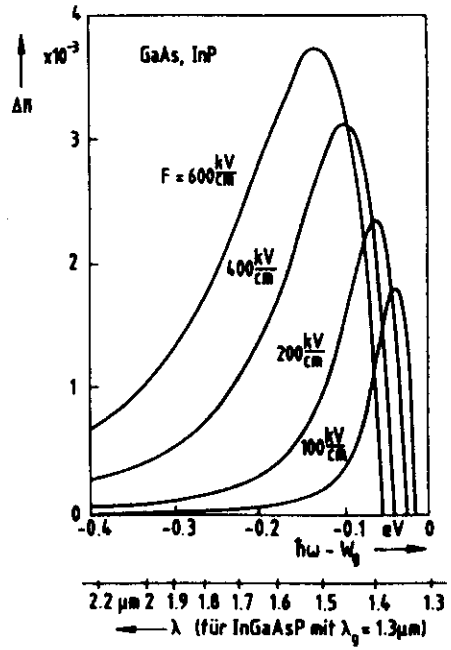

FIG. D1

E. CARRIER INJECTION

Free carriers in a material will have a strong impact on the polarization and therefore on the refractive index of a medium. Therefore, the injection of free carriers by means of a pn-junction in semiconductors may be well utilized for light modulation. Changes in the density of free carriers in the order of 10^{18} may be achieved by pn- junctions operated in the forward direction leading to changes in the refractive index by about $4\ 10^{-4}$ at $\lambda \approx 1.5\ \mu m$. Since for short devices in the order of some hundred micrometer the losses resulting from free carrier absorption can be neglected, the plasma effect may be applied for phase modulators and intensity modulators which are based on phase changes.

F. OPTICAL CONTROL

As we have seen, the excitation of valence band electrons into the conduction band changes the optical absorption of a semiconductor. This excitation may be performed not only electrically by carrier injection, but as well optically. The change of the absorption by free carriers is shown in Fig. F1. As it is known from the basics of light amplification, strong excitation of electrons into the conduction band (creation of 'inversion') will lead to bleaching of the absorption for photon energies near the band edge and even to amplification. These changes in the absorption will result in changes of the refractive index like in electrorefraction.

The chance of controlling the optical properties of matter by light opens up exciting new possibilities for all-optical modulators and switches.

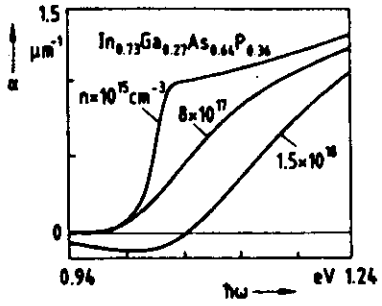

FIG. F1

G. QUANTUM CONFINED STARK EFFECT

In very thin semiconductor films (e.g. 20 nm) the density of states normal the the film planes is not continuous, but has a quantum structure. These films are so called quantum films. If a static electrical field is applied normal to a quantum film, the band edges and the potential wells are tilted (Fig. G1) - similar to the Franz-Keldysh effect. By this deformation the energy levels of the bound electrons and holes will be shifted towards lower differences between their energy levels. Consequently, the absorption edge is shifted towards longer wavelengths (Fig. G2). Since the change of the energy levels of an atomic system under the influence of strong electrical fields is known as Stark-effect, this effect in quantum films - which is much stronger than the classical Franz-Keldysh-effect - is called quantum confined Stark-effect (QCSE).

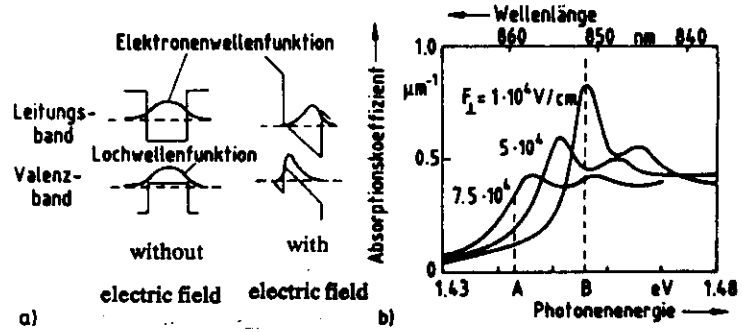

FIG. G1

IV. GUIDED - WAVE DEVICES FOR MODULATION AND SWITCHING

The fundamental principal of guided wave or integrated optics is the confinement of light in films or channels by the principal of total internal reflection. This condition may be fullfilled, if the index of refraction of the light guiding medium is higher than that of the surrounding. Fig. IV-1 illustrates the side-view of a slab waveguide (n_f, n_s, n_c are the film, substrate and cover refractive indices) showing the zig-zag propagation of the light path by total internal reflection from both interfaces.

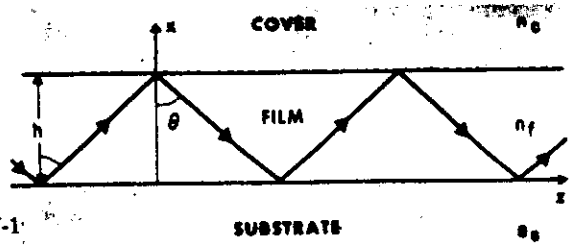

Fig. IV-1

The advantage of using waveguide configurations for optical modulation and switching lies in the fact that the light confined in a waveguide can travel in a very limited cross-sectional area over an essentially unlimited interaction length in contrast to bulk modulators, where the maximum interaction length is determied by defraction effects (see at 'Geometrical considerations' of electrooptic modulators). This results in low modulation voltages and, because of the small interaction volume, to large savings in the modulation power.

A. ELECTROOPTIC SWITCHES AND MODULATORS IN $LINBO_3$

In integrated optics, components based on $LiNbO_3$ are the most advanced with respect to performance (insertion loss, modulation power, speed, complexity) and commercialization. This progress has been achieved by improvements made in the development of the substrate material quality (homogenity, control of stoichiometry, impurity content), in the waveguide fabrication technology (titanium indiffusion and proton exchange), and in the modelling capabilities. The high status of integrated optic devices in $LiNbO_3$ may be characterized by intensity modulators with a bandwidth up to 40 GHz, complex switch arrays with 64 switches integrated on one substrate, high-speed low-insertion-loss PSK-modulators for coherent systems, and fibre-coupled devices with insertion loss figures less than 1 dB. Furthermore, there has been considerable progress in fibre-pigtailing and packaging of $LiNbO_3$ chips as well as in improving the DC- and environmental stability.

✱ Copy from R.C.Alferness, "Titanium-diffused Lithium Niobate Waveguide Devices" in T. Tamir (Ed.), Guided-Wave Optoelectronics, Springer Series in Electronics and Photonics 26, Springer, 1988, pp 145

4.3 Switch/Modulator ✱

Optical switches are required for signal routing. Applications include switching of wide-band services, protecction and facility switching in lightwave networks and bypass switching in local area networks. Signal-processing application includes programmable delay lines. In addition, high-speed switches may be used for time-division multiplexing to allow several lower bit rate channels to cooperatively utilize the high bandwidth of a common single-mode fiber and as external modulators for signal encoding. The most basic optical switch must have at least two usable output ports and, for symmetry, two input ports are also desirable. Important switch parameters include the required switching voltage, crosstalk of the two switch states and optical insertion loss. For time-division multiplexing and signal encoding, the switching speed is also important. Several switch types – the directional coupler, the balanced bridge interferometer and the intersecting waveguide switch – have demonstrated two low crosstalk switching states. In addition, branching-type switches have been covered in Chap. 3.

4.3.1 Directional Coupler

The directional coupler is a very versatile device geometry. This device, in several forms, has been used to provide many functions like wavelength filtering and polarization selection, as discussed later. It consists of a pair of closely spaced identical strip waveguides, as shown in Fig. 4.18a. Light input to one waveguide couples into the second as a result of the overlap in the evanescent fields of the two guides. The coupling per unit length, κ, depends upon the waveguide parameters, the guided wavelength λ and the interwaveguide gap g [4.80–82]. The directional coupler is also characterized by the difference in propagation constants between the two waveguides, $\Delta\beta = 2\pi(N_2 - N_1)/\lambda$, where N are the effective indices, and by the interaction length L. The phase mismatch can be adjusted via the linear electro-optic effect by application of voltage to electrodes over or along the waveguides. Electrodes over the waveguides (Fig. 4.18) provide push/pull

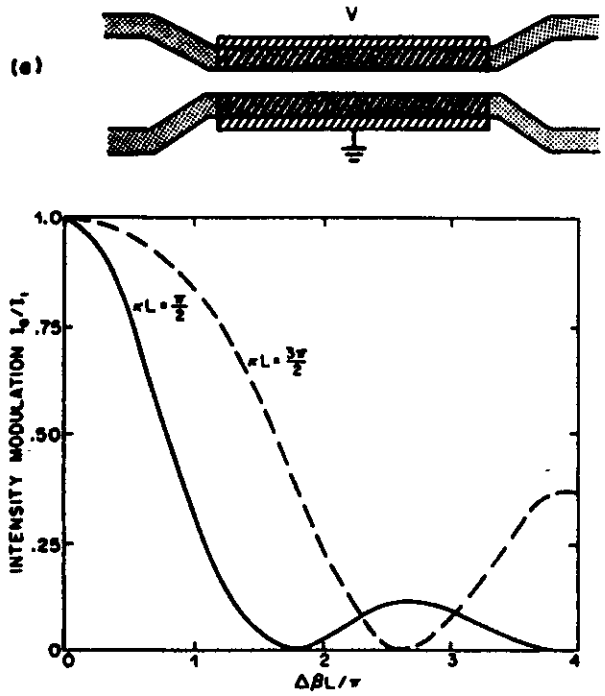

Fig. 4.18. (a) Directional coupler switch. (b) Directional coupler switch response

refractive index change between the two guides. For z-cut lithium niobate, this electrode placement utilizes the strongest electro-optic coefficient. For the x cut orientation, a three electrode configuration is required to use the r_{33} coefficient with the push/pull effect. To first order, the applied field produces only small changes in κ [4.83]. However, κ modulation has been achieved using a three electrode structure [4.84].

The operation of the directional coupler, as well as several other important Ti : $LiNbO_3$ waveguide devices, can be described by the well-known coupled-mode equations. Because of its central importance to several of the interesting Ti : $LiNbO_3$ devices, a good understanding of coupled mode theory, including the effects of weighted coupling, periodic coupling and periodic phase reversal, is essential. We therefore momentarily divert to examine the coupled-mode equations which can be written as [4.85, 86],

$$R' - j\delta R = -j\kappa S \quad , \quad \text{and} \tag{4.3.1}$$

$$S' + j\delta S = -j\kappa R \quad , \tag{4.3.2}$$

where $\delta = \Delta\beta/2$, R and S represent the complex amplitudes in the two guides (or, in general, of the two modes) and the primes represent differentiation with respect to the propagation direction. For unit input to one waveguide (or mode), the coupled intensity (efficiency) into the second waveguide (or mode) is found by solving (4.3.1, 2), which yield

$$\eta = \frac{1}{1 + (\delta/\kappa)^2} \sin^2 \kappa L [1 + (\delta/\kappa)^2]^{1/2} \quad . \tag{4.3.3}$$

For identical waveguides and no applied voltage, $\delta = 0$, $\eta = \sin^2 \kappa L$ and complete crossover occurs for $\kappa L = n\pi/2$, with n an odd integer. The length for complete coupling is $l = \pi/2\kappa$ which is called the coupling or transfer length. For $\delta \neq 0$, complete crossover is impossible regardless of the value of κL. For Ti-diffused lithium niobate waveguides, coupling lengths from $\sim 200\,\mu$m to ~ 1 cm have been demonstrated [4.81]. For the appropriate device length, the complete crossover or cross state (denoted by $\otimes$) can be achieved, in principle, without any applied voltage.

The straight through or bar state (denoted by $\ominus$) is achieved electro-optically by inducing a mismatch $\Delta\beta$ so that $\eta = 0$. To minimize the necessary $\Delta\beta L$ for 100 % modulation, a single coupling length, $l = \pi/2\kappa$, is desirable. For $\kappa L = \pi/2$, a value of $\Delta\beta L = \sqrt{3}\pi$ is required to reduce the efficiency from 100 % to 0. Multiple-coupling-length devices result in a significantly larger required $\Delta\beta L$. The switch response is shown in Fig. 4.18b; for $L \gg l$ a value of $\Delta\beta L \sim 2\kappa L$ is required for complete switching.

Reversed $\Delta\beta$ Directional Coupler

The response of the directional-coupler switch can also be modified by spatially changing $\Delta\beta$. Most important is the stepped or reversed $\Delta\beta$ coupler in which the polarity of the applied $\Delta\beta$ is periodically reversed along the interaction length [4.92, 93]. This device (Fig. 4.20) overcomes two severe limitations of the standard switched directional coupler. The first is the fabrication difficulty associated with making L exactly an integer number of coupling lengths required to assure 100 % crossover in the absence of voltage. Note that this would not be a problem if κ could be efficiently changed electro-optically. The second disadvantage is the fact that a larger value of $\Delta\beta L$ is required if L corresponds to multiple-coupling lengths. The former is more critical for switching applications where low crosstalk for both switch states is typically required. In modulators $L \neq nl$ simply results in loss on the "on" state. The second problem is more critical for high-speed modulation where low voltage is essential. An appropriately small electrode gap is desirable to reduce the drive voltage. However, for typical values of G, the

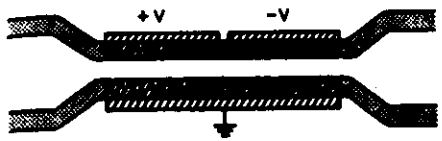

Fig. 4.20. Directional coupler with reversed $\Delta\beta$ control electrodes

transfer length l is small compared to the value of L required for acceptably low drive voltage. In this predicament, the full advantage in low values of V for longer L is not realized. However, for the reversed $\Delta\beta$ modulator as shown below, the required swing in $\Delta\beta L$ is $\sim\sqrt{3}\pi$ even for $L/l > 1$ provided that the number of electrode sections is equal to the approximate number of coupling lengths. The voltage response for the reversed $\Delta\beta$ coupler can be calculated most conveniently by multiplication of the transfer matrices for each section which are identical except for the periodic sign change of $\Delta\beta$ [4.92]. The voltage response for an N (N even) sections, $\Delta\beta$-reversed modulator can be compactly written as [4.92]

$$\eta = \sin^2 \kappa_{\text{eff}} L \quad , \quad \text{where} \tag{4.3.13}$$

$$\kappa_{\text{eff}} = \frac{N}{L} \sin^{-1} \sqrt{\eta_s} \quad . \tag{4.3.14}$$

Here η_s is the crossover efficiency of one section of length L/N given by (4.3.3). Note that perfect $\otimes$ and $\ominus$ states can be achieved for electro-optically adjustable values of $\Delta\beta$. The values of $\Delta\beta L$ required to achieve $\otimes$ and $\ominus$ states as a function of κL can be conveniently displayed in the switching curve shown in Fig. 4.21. The ordinate is the fabrication determined value of L/l while the abscissa is the (generally) electro-optically induced value of $\Delta\beta L$. The curves show the required combinations to achieve the $\otimes$

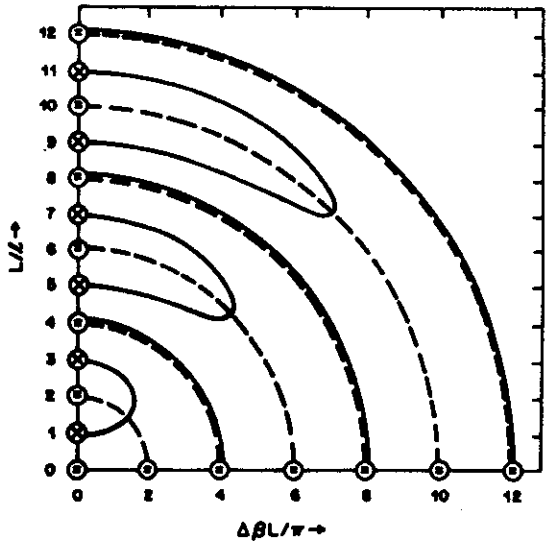

Fig. 4.21. Reversed $\Delta\beta$ switching diagram. Curves show combination of L/l and $\Delta\beta L$ values required for $\otimes$ and $\ominus$ states. Dashed curves are switching curves for $\ominus$ state of a directional coupler with uniform control electrodes. (After [4.92])

or $\ominus$ state as indicated. It is important to note again that for the uniform $\Delta\beta$ coupler $\otimes$ states can be achieved only for isolated points $L/l = 1, 3, \ldots$ on the ordinate which places generally unachievable demands upon the fabrication process. Measurement-limited crosstalk values (~ 43 dB) have been achieved with reversed $\Delta\beta$ electrodes [4.94]. The flexibility achieved with the reversed-$\Delta\beta$ technique is essential for a number of Ti : $LiNbO_3$ coupled-mode devices, in addition to the directional-coupler switch, as will be discussed below. The traveling-wave principle can be combined with that of $\Delta\beta$ reversal to achieve high-speed, low-crosstalk switching [4.95, 96].

4.3.2 Balanced-Bridge Interferometer

The balanced-bridge interferometric switch [4.97, 98], shown schematically in Fig. 4.22a, is an analog of the bulk Mach-Zehnder interferometer. Light entering either of two input waveguides is divided by a 3 dB (50/50 splitter) directional coupler; the waveguides are then sufficiently separated so that they are not coupled, then combined again by a 3 dB couper. While separated, the relative phase between the two arms can be changed via the electro-optic effect. The output crossover efficiency versus the induced phase shift can be calculated with the coupled-mode equations by cascadig the results for the 3 dB coupler, the phase-shifter section (with $\kappa = 0$), and the final 3 dB coupler. For unit input to one waveguide, the crossover efficiency

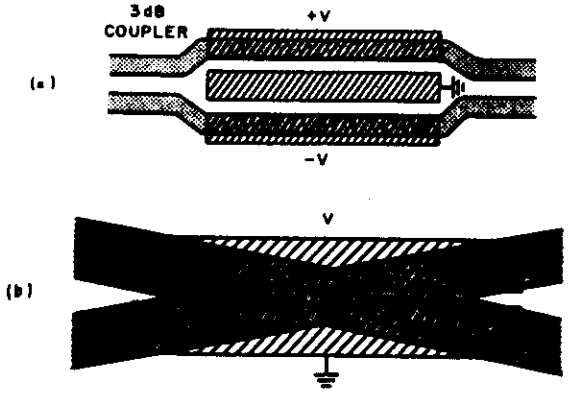

Fig. 4.22. (a) Balanced bridge interferometric switch. (b) Intersecting waveguide switch

into the second output waveguide is

$$\eta = \cos^2 \frac{\Delta\beta L}{2} \quad , \tag{4.3.15}$$

where L is the phase-shift electrode length. This switch has a periodic re-

sponse with respect to $\Delta\beta$ with multiple $\otimes$ and $\ominus$ states, in contrast to that of the switched-directional coupler but similar to the multiple-section reversed $\Delta\beta$ coupler. The required phase shift to switch from the cross to bar states is $\Delta\beta L = \pi$, which is $\sqrt{3}$ times smaller than for the directional-coupler switch. Because the efficiency depends only upon a single, voltage-controlled parameter $\Delta\beta$, both switch states can be achieved electrically.

Perfect switch states (i.e., low crosstalk) require that the splitter and combiner be perfect 3 dB couplers and that the losses in each arm be identical. For small coupler errors, $\eta = 1$ cannot be achieved. Fortunately, 3 dB couplers can be made either by fabricating such that $\kappa L = \pi/4$ and $\Delta\beta = 0$ (identical waveguides) or by making $\kappa L > \pi/4$ and electro-optically adjusting $\Delta\beta$, (4.3.3), to achieve 3 dB coupling.

Two variations of this device that use closely spaced waveguides have been reported [4.99, 100]. To eliminate coupling in the phase shift section, one uses an etched gap, the other uses mismatched waveguides. However, generally only poor crosstalk results have been achieved for these configurations. These structures do have the advantage that no bends are required, which can potentially reduce optical loss.

4.3.3 Intersecting-Waveguide Switch

Several types of intersecting-waveguide switches, one of which is shown schematically in Fig. 4.22b, have been demonstrated with $Ti:LiNbO_3$ waveguides [4.101–105]. Although an early device that employed multimode waveguides apparently operated by the principle of total internal reflection [4.104], the single-mode version can be viewed as a zero-gap directional coupler or a modal interferometer. It is convenient to study the symmetric directional coupler by considering the two eigenmodes of (Chap. 3) the total structure rather than the spatial modes of the individual waveguide as in the coupled-mode formalism [4.105]. Eigenmodes for a totally symmetric structure do not couple but propagate with different phase velocities. Coupling light into either well-separated input waveguide equally excites the two normal modes, which propagate through the structure unperturbed but interfere based upon their different modal path lengths. The latter can be altered with a symmetric transverse electro-optic field to change the relative output amplitudes in the two output waveguides. Because it is an interferometer, ideally both switch states can be achieved with low crosstalk. However, to achieve that, the structure both with and without applied fields must be symmetric to avoid coupling between the local normal modes to insure good modal interference and resulting low switch crosstalk. By careful fabrication, electrode design and alignment, crosstalk approaching −30 dB has been achieved. These switches exhibit voltage times length products comparable to finite gap directional coupler switches [4.106].

POLARIZATION INDEPENDENT SWITCHES

The $LiNbO_3$ electrooptic switches described in the previous section generally show a strong polarization dependence. In the field of optical switching, however, polarization independence is highly desired, since optical switches or switching networks should be applicable to usual telecommunication systems and, therefore, they should be compatible with standard single mode fibres. A number of polarization independent switches has been proposed and demonstrated. However, most of them had some severe drawbacks with respect to fabrication tolerances, crosstalk, switching voltage, etc. Only in recent time considerable progress has been made in the development of manufacturable polarization independent switches with reduced fabrication tolerances. Two concepts which meet these requirements are the balanced bridge interferomertic switch whith light propagation in Z-direction and the so called "digital optical switch".

The digital optical switch is called "digital", because it has a steplike transferfunction (see Fig.). Both polarizations are switched, if the applied voltage is high enough. The reason for this behavior is that this switch is not an interferometric one like the directional couplers, the BOA- and X-switches, and the above mentioned balanced bridge switches. The digital optical switch is based on an electrooptically induced break of the symmetry of an adiabatic waveguide transition and utilizes the mode sorting effect of asymmetric waveguide transitions. By this mean, the fundamental mode excited at the input Y-junction can be switched to the desired output port. Although the electrooptic coefficients

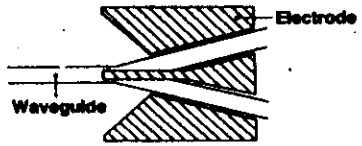

Digital Optical Switch

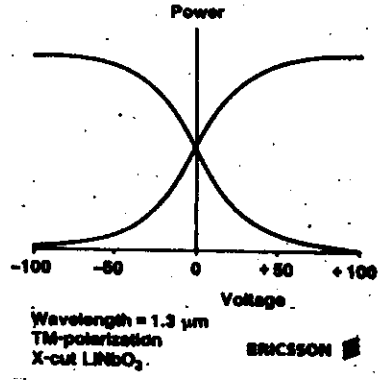

Measured Transfer Function

for both polarizations are generally not identical, polarization independence is achieved by increasing the voltage sufficiently. Polarization independent operation of the digital switch has been demonstrated for voltages of ±60 V and a resulting crosstalk of 14 dB. Besides the polarization independence, the main advantage of the switch is its tolerance against fluctuations of the applied voltages. Therefore all switches e.g. in a switch array may be operated by the same switching voltage. Furthermore, moderate DC- drift effects will not deteriorate the switch performance.

4.4 On/Off Modulators *

High-speed waveguide intensity modulators may be essential components for very-high-bit-rate lightwave systems. Direct current modulation of semiconductor lasers is the most convenient and presently used method for data encoding for data rates to ~2 Gigabit/s. However, in most semiconductor lasers fast current modulation also results in an undesirable wavelength modulation or chirp which limits bandwidth for propagation at the lowest-loss region of the standard silica fiber $\lambda = 1.55\,\mu$m, where finite dispersion is encountered. External modulation eliminates chirp to allow longer-distance transmission. We will examine this application in more detail later.

An on/off modulator is inherently more simple than a 2×2 switch because only a single usable output port is required. In addition to the switches mentioned above, electro-optic $Ti:LiNbO_3$ on/off waveguide modulators based upon Y branch interferometers [4.51, 97, 108–110], active Y branching [4.111], induced waveguide cutoff [4.112], and TE ↔ TM mode conversion [4.113, 114] have been demonstrated. Important modulator characteristics are the modulation depth or on/off extinction ratio, required drive voltage and the modulator speed or bandwidth. An extinction ratio of ~15 dB is generally considered sufficient.

4.4.1 Y-Branch Interferometer

The Y-branch interferometer, which operates by the same principle as the balanced-bridge modulator, is shown in Fig. 4.23. However, unlike the balanced-bridge switch, it has only a single accessible input and output port. It

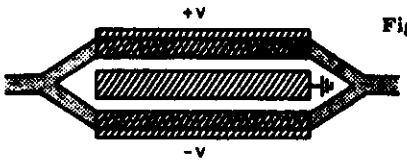

Fig. 4.23. Y-branch interferometric modulator

* Copy from R.C.Alferness, "Titanium-diffused Lithium Niobate Waveguide

has been an especially popular structure for on/off modulation because of its simplicity. The 3 dB splitter and combiner are power splitting Y branches. The input wave in split into equal components. Each propagates over one arm of the interferometer. The interferometer waveguide arms are sufficiently separated to prohibit evanescent coupling between them and thus are not coupled. The optical paths of the two arms are typically equal. Therefore if no phase shift is introduced between the interferometer arms, the two components combine in phase at the output Y-branch 3 dB coupler and continue to propagate undiminished in the output waveguide. For $\Delta\beta L = \pi$, however, the combined mode distribution is double-mode-like; light is radiated into the substrate and the transmitted light is a minimum. The transmission-efficiency response is the same as for the balanced-bridge switch/modulator. A three-electrode configuration can be used to achieve a push-pull phase change; however the capacitance is then also increased, which is disadvantageous when high-speed operation is desired. For modulator applications the interferometer is typically dc biased for 50 % transmission and an ac modulation signal added. Bias can be achieved either electro-optically by an applied bias voltage or optically by using interferometer arms of slightly different length [4.115].

A variation of this device is to use an asymmetric branch on the output side of the interferometer to provide two usable output ports thus converting it to a one by two switch [4.115a].

Other types of waveguide intensity modulators include the cutoff, and polarization modulators. The cutoff modulator is simply a phase modulator in which the induced index change reduces the waveguide-substrate index so that guiding is eliminated and light radiates into the substrate. Its principal advantage is its simplicity. However, for a low modulation voltage, the waveguide must be near cutoff which usually implies significant optical loss for the on ($V = 0$) state. Furthermore, this condition requires careful control of waveguide parameters. The polarization modulator will be discussed in a later section.

4.4.2 Voltage and Bandwidth Consideration for Switch/Modulators

The expected voltage x length product for directional coupler and interferometric type switch/modulators can be determined from (4.2.10) with $p = \sqrt{3}$ and 1, respectively. Experimentally, VL for directional coupler

switches using z-cut Ti:$LiNbO_3$ waveguides scales as λ^2 and can be written as $VL \sim 3.2\,\mathrm{V\,cm}\ \lambda^2$ with λ in units of μm [4.116].

The electrical frequency response results from phase modulators, for both the lumped and traveling-wave (TW) cases, translate directly to those for interferometric modulators because the amplitude modulation depends simply upon the integrated phase change. The same is true for the lumped directional-coupler device. However, the situation is quite different for the TW directional coupler where the distribution of $\Delta\beta$ along the coupler, not just its integrated value, is important. For example, for a directional coupler modulator with $L = l$, the phase mismatch at either end of the coupler, where most of the light is in only one of the waveguides, is relatively unimportant. Physically the effect of velocity mismatch is weighted along the coupler and is most critical at the center of the coupler and least sensitive at the ends. As a result, with respect to velocity mismatch the effective coupler length is shorter, $\sim L/\sqrt{3}$, than the actual length [4.117, 118]. The result is that for equal interaction lengths, directional-coupler modulators provide greater velocity-mismatch limited bandwidth than interferometric ones. Indeed, this increase in bandwidth is approximately equal to the increase in drive voltage required for the directional coupler compared to the interferometer. Calculated frequency responses for the two modulator types are shown in Fig. 4.24. The effective weighting between the optical and electrical signals in the case of the directional coupler results in low sidelobes of the frequency response.

Numerous demonstrations of very broadband interferometric and directional coupler modulators have now been reported [4.39, 40, 119–122]. Applications will be discussed later.

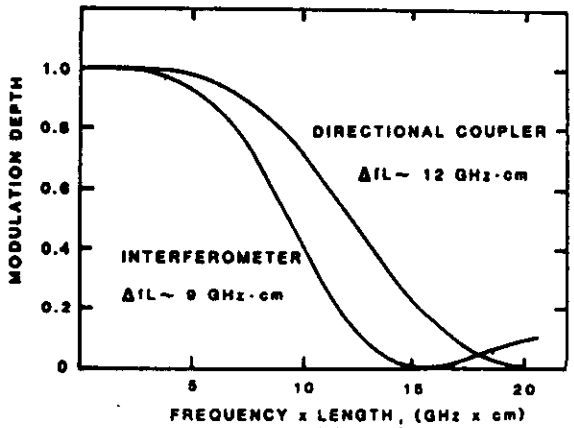

Fig. 4.24. Calculated optical modulation frequency response for traveling-wave interferometric and directional coupler modulators. (After [4.117])

B. GUIDED-WAVE ACOUSTO-OPTIC DEVICES

✱ Copy from A.Yariv, P.Yeh, "Optical waves in crystals", John Wiley, New York, 1984, pp 386

10.2.2. Surface Acousto-optic Beam Deflectors ✱

Bragg interactions have recently been demonstrated [11] between surface acoustic waves and optical guided waves (see Chapter 11) in thin-film dielectric waveguides. Since the diffraction efficiency η depends, according to Eq. (10.1-11), on the acoustic intensity I_a, the confinement of the acoustic power near the surface (to a depth $\sim \Lambda$) leads to low modulation or switching power. Figure 10.9 shows an experimental setup in which both the surface wave and the optical wave are guided in a single crystal of $LiNbO_3$. The dielectric waveguide is produced by out-diffusion of Li from a layer of $\sim 10\ \mu$m near the surface, which raises the index of refraction. Figure 10.10 shows the deflected light spots as the acoustic frequency was varied in a beam deflector using three tilted-surface acoustic-wave transducers [13]. A random access time τ of 1.24 μs and a bandwidth of 358 MHz were obtained, which correspond to 400 resolvable spots.

The surface acousto-optic beam deflector is used as a key element in the RF spectrum analyzer (see Section 10.4).

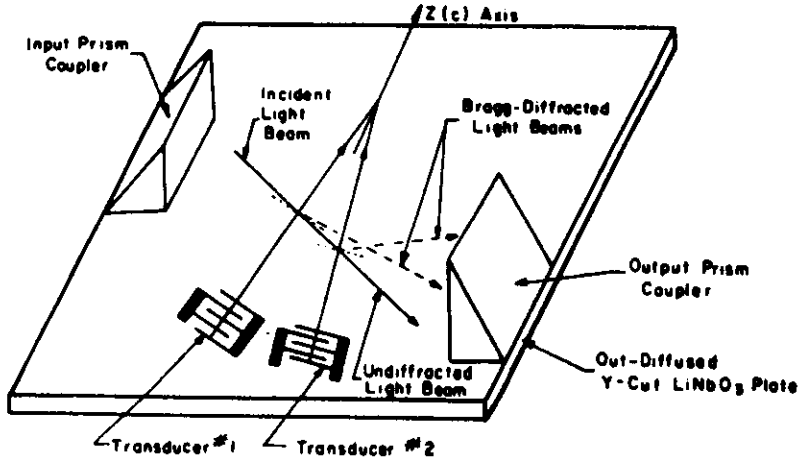

Figure 10.9. Guided-wave acousto-optic Bragg diffraction from two tilted surface acoustic waves [12].

Acousto-optic tunable filter

Important components in high dense wavelenght division multiplexed systems are tunable narrow-band optical filters. Such filters can be realized in integrated form by the high wavelength selectivity of the polarization coupling induced by surface acoustic waves. Polarization independent acousto-optic tunable filters have been fabricated by two integrated polarization splitters (at the in- and output) and by two polarization converters driven by surface acoustic waves. The optical bandwidth is in the order of 1 nm and the tuning range about 100 nm. Therefore narrow optical bandwidth and broad tuning range can be combined by this device.

POLARIZATION INDEPENDENT
ACOUSTO-OPTIC TUNABLE FILTER

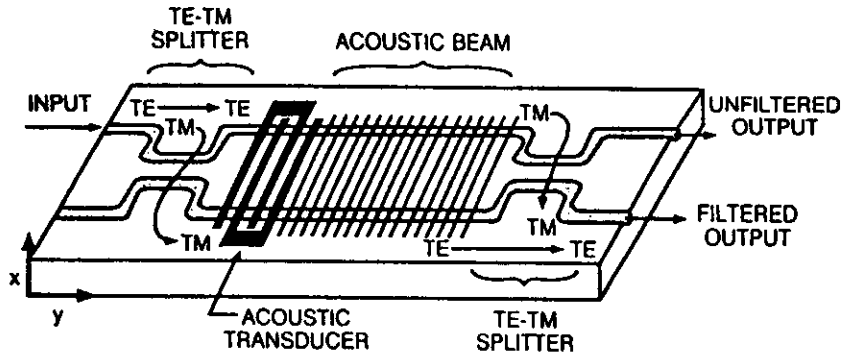

C. SEMICODUCTOR DEVICES

1. Electroabsorption modulator

Fig. C-1 shows the front end view of a typical AlGaAs-electroabsorption modulator and the voltage dependent transmission. The strip loaded film waveguide contains a pn-junction. Without applied voltage, light at λ = 790 nm is transmitted through the 350 μm long waveguide practically without losses. If an electrical field is applied in reverse direction, losses will increase because of the Franz Keldish effect. The dynamic of the modulator is determined by the electrical RC time constant.

Fig. C-1

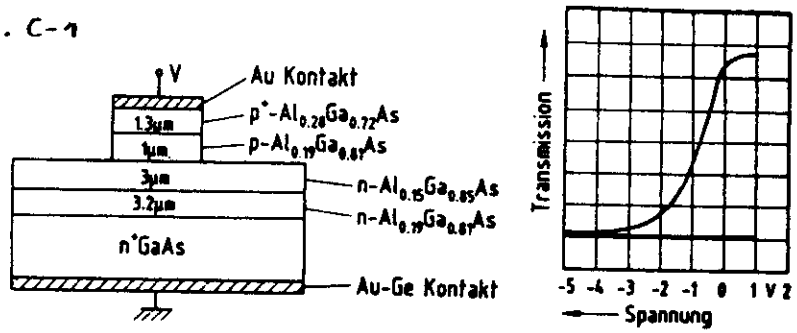

2. Carrier injection X-switch

The switch shown in Fig. C-2 is similar to the $LiNbO_3$ intersecting waveguide switch except that here the control of the relative phase difference between the two modes excited in the intersection region is performed by the plasma effect. The free carriers are injected by a pn-junction.

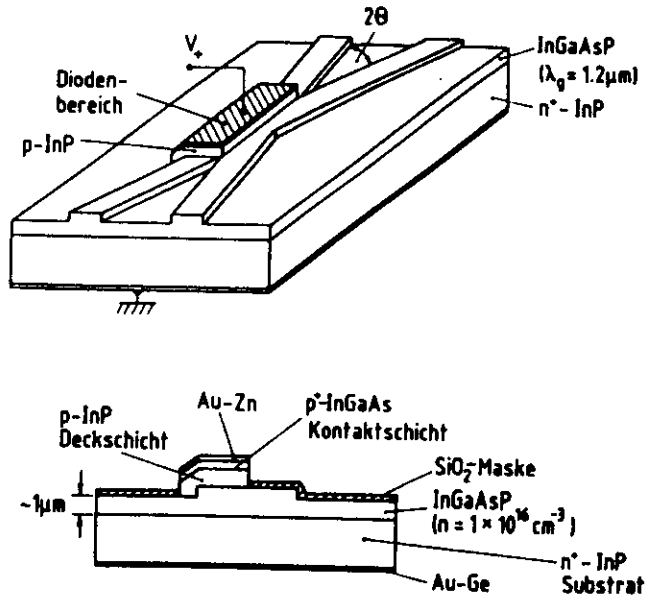

Fig. C-2

REFERENCES "SWITCHING AND MODULATION"

A. GENERAL

1. A. Yariv, P.Yeh, "Optical Waves in Crystals", John Wiley, New York, 1984
2. H. A. Haus, "Waves and Fields in Optoelectronics", Prentice Hall, New Jersey, 1984

B. ELECTROOPTICS

1. I.P.Kaminow, "An Introduction to Electrooptic devices", Academic Press, New York, 1974
2. I.P.Kaminow, E.H.Turner, "Electrooptic light modulators", Proceedings of the IEEE, vol. 54, 1966, pp 1374

C. ACOUSTOOPTICS

1. A. Korpel, "Acoustooptics", Marcel Dekker, New York, 1988
2. I.C.Chang, "Acoustooptic devices and applications", IEEE Trans. SU-23, (1976), pp 2-22

D. GUIDED-WAVE OPTICAL MODULATORS AND SWITCHES

1. General

1. T.Tamir (Ed.), "Integrated Optics", Topics in Applied Physics, vol. 7, Springer, Berlin, 1985
2. T.Tamir (Ed.), "Guided-Wave Optoelectronics", Springer Series in Electronics and Photonics 26, Springer, Berlin, 1988
3. R.G.Hunsperger, "Integrated Optics: Theory and Technology", Springer Series in Optical Sciences 33, Springer, Berlin, 1984

2. Electrooptic devices utilizing $LiNbO_3$

1. R. C. Alferness, "Waveguide Electrooptic Modulators," IEEE Transactions on Microwave Theory and Techniques, Vol. MTT-30, pp. 1121-1137, August, 1982.
2. E. Voges and A. Neyer, "Integrated-Optic Devices on $LiNbO_3$ for Optical Communication," Journal of Lightwave Technology, Vol. LT-5, pp. 1229-1238, September, 1987.
3. R. V. Schmidt and I. P. Kaminow, "Metal-diffused Optical Waveguides in $LiNbO_3$," Applied Physics Letters, Vol. 25, pp. 458-460, October, 1974.
4. M. Papuchon, Y. Combemale, X. Mathieu, D. B. Ostrowsky, L. Reiber, A. M. Roy, B. Sejourne and M. Werner, "Electrically Switched Optical Directional Coupler: Cobra," Applied Physics Letters, Vol. 27, pp. 289-291, September, 1975.

5. H. Kogelnik and R. V. Schmidt, "Switched Directional Couplers with Alternating ," IEEE Journal of Quantum Electronics, Vol. QE-12, pp. 396-401, July, 1976.
6. M. Papuchon, A. Roy and D. B. Ostrowsky, "Electrically Active Optical Bifurcation: BOA," Applied Physics Letters, Vol. 31, pp. 266-267, August, 1977.
7. W. K. Burns, T. G. Giallorenzi, R. P. Moeller, and E. J. West, "Interferometric Waveguide Modulator with Polarization Independent Operation," Applied Physics Letters, Vol. 33, pp. 944-947, December, 1978.
8. R. C. Alferness, "Optical Directional Couplers with Weighted Coupling," Applied Physics Letters, Vol. 35, pp. 260-262, August, 1979.
9. R. C. Alferness, "Efficient Waveguide Electro-Optic TE TM Mode Converter/Wavelength Filter," Applied Physics Letters, Vol. 36, pp. 513-515, April, 1980.
10. J. L. Jackel, V. Ramaswamy and S. P. Lyman, "Elimination of Out-Diffused Surface Guiding in Titanium-Diffused $LiNbO_3$," Applied Physics Letters, Vol. 38, pp. 509-511, April, 1981.
11. J. L. Jackel, C. E. Rice, and J. J. Veselka, "Proton Exchange for High-Index Waveguides in $LiNbO_3$," Applied Physics Letters, Vol. 41, pp. 607-608, October, 1982.
12. G. T. Harvey, "The Photorefractive Effect in Directional Coupler and Mach-Zender $LiNbO_3$ Optical Modulators at Wavelength of 1.3um," Journal of Lightwave Technology, Vol. 6, pp. 872-876, June, 1988.
13. P. Granestrand, B. Stoltz, L. Thylen, K. Bergvall, W. Doldissen, H. Heinrich and D. Hoffmann, "Strictly Nonblocking 8 X 8 Integrated Optical Switch Matrix," Electronics Letters, Vol. 22, pp. 816-818, July, 1986.
14. Y. Silberberg, P. Perlmutter and J. E. Baran, "Digital Optical Switch," Applied Physics Letters, Vol. 51, pp. 1230-1232, October, 1987.
15. F. J. Leonberger, "High-Speed Operation of $LiNbO_3$ Electro-Optic Interferometric Waveguide Modulators," Optics Letters, Vol. 5, pp. 312-314, July, 1980.
16. R. A. Becker, "Traveling-Wave Electro-Optic Modulator with Maximum Bandwidth-Length Product," Applied Physics Letters, Vol. 45, pp. 1168-1170, December, 1984.
17. S. K. Korotky, G. Eisenstein, R. S. Tucker, J. J. Veselka and G. Raybon, "Optical Intensity Modulation to 40 GHz Using A Waveguide Electro-Optic Switch," Applied Physics Letters, Vol. 50, pp. 1631-1633, June, 1987.

3. Acoustooptic devices

1. C.S.Tsai, "Guided-Wave Acousto-Optics", Springer Series in Electronics and Photonics 23, Springer, Berlin, 1990

4. Semiconductor devices

1. T. H. Wood, "Multiple Quantum Well (MQW) Waveguide Modulators," Journal of Lightwave Technology, Vol. 6, pp. 743-757, June, 1988.

2. S. Y. Wang, and S. H. Lin, "High Speed III-V Electrooptic Waveguide Modulators at = 1.3 m," Journal of Lightwave Technology, Vol. 6, pp. 758-771, June, 1988.

3. S. Somekh, E. Garmire, A. Yariv, H. L. Garvin and R. G. Hunsperger, "Channel Optical Waveguides and Directional Couplers in GaAs-Imbedded and Ridged," Applied Optics, Vol. 13, pp. 327-330, February, 1974.

4. F. J. Leonberger and C. O. Bozler, "GaAs Directional-Coupler Switch With Stepped Reversal," Applied Physics Letters, Vol. 31, pp. 223-226, August, 1977.

5. H. Inoue, K. Hiruma, K. Ishida, T. Asai and H. Matsumura, "Low Loss GaAs Optical Waveguides," Journal of Lightwave Technology, Vol. LT-3, pp. 1270-1276, December, 1985.

6. U. Koren, B. I. Miller, T. L. Koch, G. D. Boyd, R. J. Capik and C. E. Soccolich, "Low Loss InGaAs/InP Multiple Quantum Well Waveguides," Applied Physics Letters, Vol. 49, pp. 1602-1604, December, 1986.

7. J. P. Donnelly, N. L. DeMeo, G. A. Ferrante and K. B. Nichols, "A High-Frequency GaAs Optical Guided-Wave Electrooptic Interferometric Modulator," IEEE Journal of Quantum Electronics, Vol. QE-21, pp. 18-21, January, 1985.

8. P. Buchmann, H. Kaufmann, H. Melchior, and G. Guekos, "Broadband Y-Branch Electro-optic GaAs Waveguide Interferometer for 1.3 m," Applied Physics Letters, Vol. 46, pp. 462-464, March 1985.

9. R. G. Walker, "High-Speed Electrooptic Modulation in GaAs/GaAlAs Waveguide Devices," Journal of Lightwave Technology, Vol. LT-5, pp. 1444-1453, October, 1987.

10. L. A. Coldren, J. G. Mendoza-Alvarez and R. H. Yan, "Design of Optimized High-Speed Depletion-Edge-Translation Optical Waveguide Modulators in III-V Semiconductors," Applied Physics Letters, Vol. 51, pp. 792-794, September, 1987.

11. K. Ishida, H. Nakamura, H. Matsumura, T. Kadoi, and H. Inoue, "InGaAsP/InP Optical Switches Using Carrier Induced Refractive Index Change," Applied Physics Letters, Vol. 50, pp. 141-142, January, 1987.

12. J. S. Weiner, D. A. B. Miller, D. S. Chemla, T. C. Damen, C. A. Burrus T. H. Wood, A. C. Gossard, and W. Wiegmann, "Strong Polarization-Sensitive Electroabsorption in GaAs/AlGaAs Quantum Well Waveguides," Applied Physics Letters, Vol. 47, pp. 1148-1150, December, 1985.

13. H. Soda, K. Nakai, H. Ishikawa, and H. Imai, "High-Speed GaInAsP/InP Buried-Heterostructure Optical Intensity Modulator with Semi-Insulating InP Burying Layers," Electronics Letters, Vol. 23, pp. 1232-1234, November, 1987.

Additional Applications

1. H. F. Taylor, "Application of Guided-Wave Optics in Signal Processing and Sensing," Proceedings of the IEEE, Vol. 75, pp. 1524-1535, November, 1987.

2. C. S. Tsai, "Guided-Wave Acoustooptic Bragg Modulators for Wide-Band Integrated Optic Communications and Signal Processing," IEEE Transactions on Circuits and Systems, Vol. CAS-26, pp. 1072-1098, December, 1979.

3. C. M. Verber, R. P. Kenan and J. R. Busch, "Correlator Based On An Integrated Optical Spatial Light Modulator," Applied Optics, Vol. 20, pp. 1626-1629, May, 1981.

4. D. B. Anderson, J. T. Boyd, M. C. Hamilton, and R. R. August, "An Integrated-Optical Approach to the Fourier Transform," IEEE Journal of Quantum Electronics, Vol QE-13, pp. 268-275, April, 1977

5. D. Mergerian, E. C. Malarkey, R. P. Pautienus, J. C. Bradley, G. E. Marx, L. D. Hutcheson and A. L. Kellner, "Operational Integrated Optical R. F. Spectrum Analyzer," Applied Optics, Vol. 19, pp. 3033-3034, September, 1980.

6. L. Thylen, "Integrated Optics in $LiNbO_3$: Recent Developments in Devices for Telecommunications," Journal of Lightwave Technology, Vol. 6, pp. 847-861, June, 1988.

7. S. K. Korotky, G. Eisenstein, A. H. Gnauck, B. L. Kasper, J. J. Veselka, R. C. Alferness, L. L. Buhl, C. A. Burrus, T. C. D. Huo, L. W. Stulz, K. C. Nelson, L. G. Cohen, R. W. Dawson, and J. C. Campbell, "4-Gb/s Transmission Experiment over 117 km of Optical Fiber Using A Ti:$LiNbO_3$ External Modulator," Journal of Lightwave Technology, Vol. LT-3, pp. 1027-1031, October, 1985.

8. C. Schaffer and G. Stock, "Integrated Optical Circuit for Fibre Gyroscope Applications," Electronics Letters, Vol. 24, pp. 1357-1358, October, 1988.

9. B. L. Heffner, D. A. Smith, J. E. Baran, A. Yi-Yan, and K. W. Cheung, "Integrated-Optic Acoustically Tunable Infra-Red Optical Filter," Electronics Letters, Vol. 24, pp. 1562-1563, December, 1988.

10. C. H. Bulmer, "Sensitive, Highly Linear Lithium Niobate Interferometers for Electromagnetic Field Sensing," Applied Physics Letters, Vol. 53, pp. 2368-2370, December, 1988.